Urban Climate 37 (2021) 100817

Contents lists available at ScienceDirect

Urban Climate

journal homepage: www.elsevier.com/locate/uclim

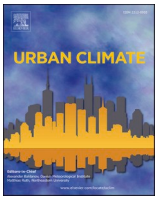

Evaluation and application of a low-cost measurement network to study intra-urban temperature differences during summer 2018 in Bern, Switzerland

Moritz Gubler [a,b,c,*], Andreas Christen [d], Jan Remund [e], Stefan Brönnimann [a,c]

[a] Climatology, Institute of Geography, University of Bern, Bern 3012, Switzerland
[b] Institute for Lower Secondary Education, Bern University of Teacher Education, Bern 3012, Switzerland
[c] Oeschger Centre for Climate Change Research, University of Bern, Bern 3012, Switzerland
[d] Chair of Environmental Meteorology, Institute of Earth and Environmental Sciences, Faculty of Environment and Natural Resources, University of Freiburg, Freiburg 79085, Germany
[e] Meteotest AG, Bern 3012, Switzerland

ARTICLE INFO

Keywords:
Urban climate
Urban heat island
Air temperature
Low-cost
Radiation shield
Measurement network

ABSTRACT

The understanding of intra-urban air temperature variations is crucial to assess strategies for cities' adaptation to impacts of present and future anthropogenic climate change. Depending on extensive measurement networks, high-resolution air temperature measurements in urban environments are challenging due to high instrumentation and maintenance costs. Here, we present a low-cost measurement device (LCD) consisting of a temperature logger and a custom-made, naturally ventilated radiation shield. Besides intercomparisons with automated weather stations (AWS) at three reference sites during record-dry summer 2018, we tested the potential of the devices using a network of 79 LCDs to assess the intra-urban variability of urban heat island (UHI) patterns in the city of Bern, Switzerland. We found positive mean measurement biases between LCDs and AWS of 0.61 to 0.93 K (RMSE: 0.78 to 1.17 K) during daytime, of which up to 82.8% of the variance could be explained statistically by solar irradiance (radiative heating) and wind speed (insufficient ventilation). During night, average measurement biases were markedly lower and eventually negative with −0.12 to 0.23 K (RMSE: 0.19 to 0.34 K). Our results highlight the importance of sensor intercomparisons being conducted at multiple locations with differing urban land-cover, structure, and metabolism given that biases varied considerably between the reference sites. Data retrieved by the city-wide measurement network showed that the LCD approach is well suited for the analysis of spatiotemporal UHI patterns during night and adds considerable value compared to the few existing AWS in detecting fine-scale air temperature variability. In conclusion, the current LCD measurement approach represents a valuable option for cost-effective analyses of urban air temperature variability across multiple scales, which may be of particular value for the development, appliance, and monitoring of adaptation strategies to climate change in cities with restricted financial resources.

* Corresponding author at: Institute of Geography, Hallerstrasse 12, Bern 3012, Switzerland.
E-mail address: moritz.gubler@giub.unibe.ch (M. Gubler).

https://doi.org/10.1016/j.uclim.2021.100817
Received 9 June 2020; Received in revised form 17 January 2021; Accepted 5 March 2021

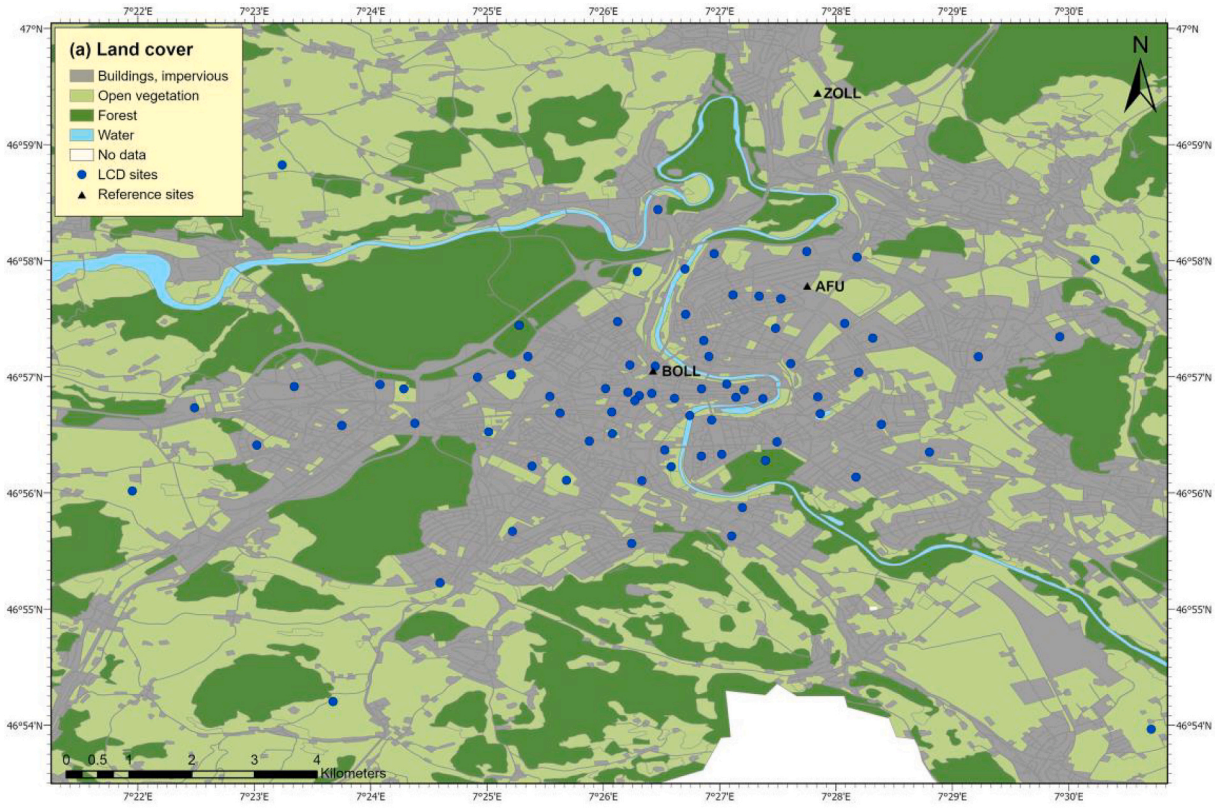

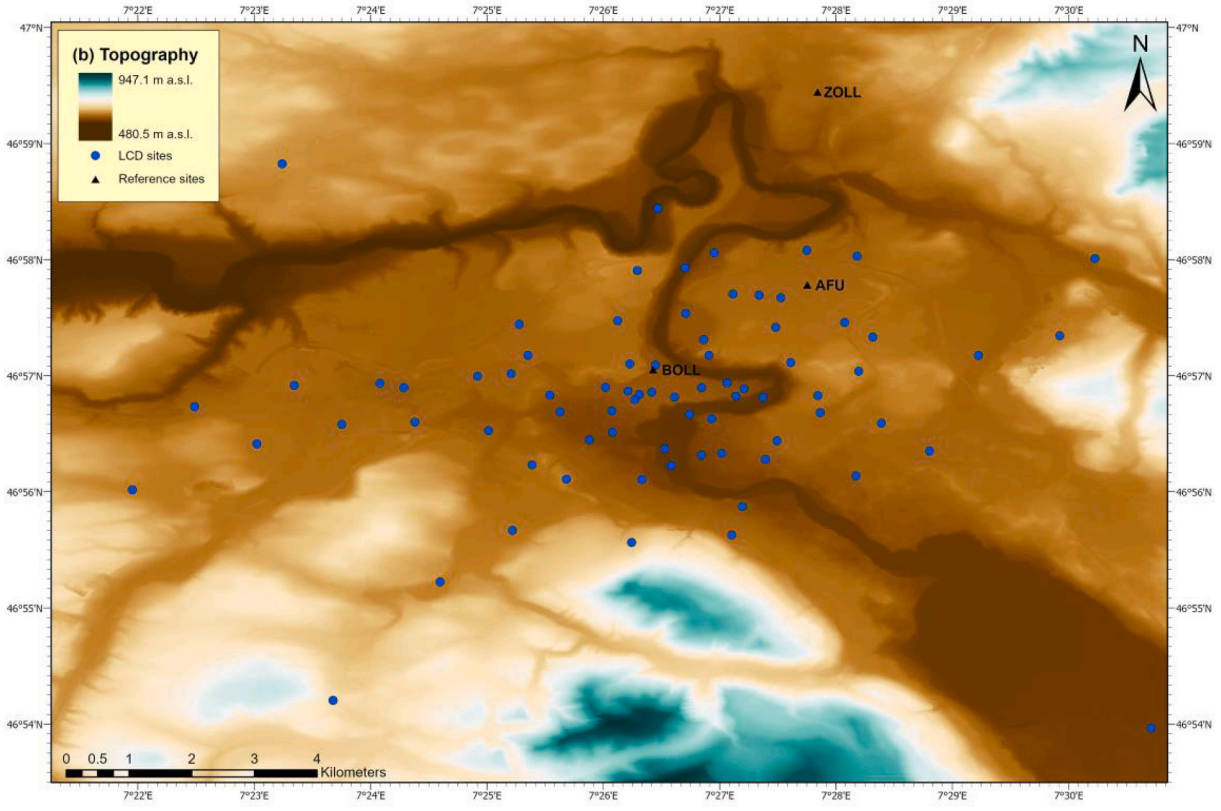

(caption on next page)

Fig. 1. Overview of a) land-cover (Urban Atlas; EEA, 2012) and b) topography (swissALTI^{3D}; Swisstopo, 2017) of the study area. The 76 LCD sites of the measurement network (blue circles) as well as the three AWS reference sites ZOLL, AFU, and BOLL (black triangles) are shown. Map coordinates refer to the World Geodetic System 1984 (WGS84), which was used for the map projection in ArcGIS Pro 2.4.0 (Esri, 2019).

1. Introduction

In the face of anthropogenic climate change, urban environments are particularly vulnerable for present and future changes in temperature extremes. The effects of projected increases in intensity, duration, and frequency of heatwaves (IPCC, 2014) are amplified in cities by the well-studied urban heat island (UHI) effect (e.g., Stewart, 2011), which adds additional thermal stress to urban populations (Milan and Creutzig, 2015; Ward et al., 2016). The planning, development, and implementation of adequate, site-specific mitigation strategies for urban heat stress requires high-resolution information about spatiotemporal patterns of UHI intensities. However, in-situ observations at fine scales are often scarce in urban environments due to relatively high costs for instrumentation, deployment, and maintenance of meteorological stations (Muller et al., 2013b). Hence, meteorological measurements in cities are in many cases limited to a few sites that may not represent the complexity of smaller-scale temperature variability across the multitude of microclimates within the urban canopy layer (Stewart and Oke, 2012), which is defined as the air volume contained between the ground and the upper limit of urban roughness elements such as buildings or trees (Oke et al., 2017).

With advances in technology, the availability of low-cost and small-sized environmental sensors with adequate accuracy has revealed new potentials regarding the assessment of near-surface atmospheric data at small spatial scales across different research disciplines (e.g., Matese et al., 2009; Young et al., 2014; Gubler et al., 2018). Allowing for more sensors to be acquired at a lower cost, it is nowadays possible to maximize spatial resolution of point-based measurements of near-surface atmospheric variables. In the field of ecology, instrumentation with costs of less than ~$50 USD per sensor is widely used for the assessment of key environmental variables such as near-surface air temperature (Gubler et al., 2018; Terando et al., 2017). With regard to existing urban meteorological networks and past UHI investigations (Grimmond, 2006; Muller et al., 2013b), studies focusing on the use and evaluation of low-cost measurement equipment are underrepresented in urban climatology. Compared to other cost-effective data acquisition methods, a carefully designed network of numerous low-cost sensors may not only overcome limitations due to spatial or temporal resolution known from remote-sensing approaches (Zhou et al., 2019), but can also avoid issues such as missing metadata or inadequate sensor installation that have been reported from approaches using crowd-sourced data (Chapman et al., 2017; Meier et al., 2017; Fenner et al., 2017, 2019). Conversely, the existence of high-resolution meteorological data offers great potential for the validation of urban climate model outputs or for data quality assessments of citizen science projects (Grimmond, 2006; Young et al., 2014).

Despite its advantages, the use of low-cost instrumentation is challenging due to the need for in-depth evaluation of data quality and potential sources of measurement errors (Meier et al., 2017; Napoly et al., 2018). Besides adequate measurement accuracy of the sensors used, potential biases emerging from radiation errors that may artificially heat or cool the sensors' surrounding air require proper shielding of the sensor (WMO, 2014). In comparison to potential daytime biases, when incoming solar irradiance dominates the radiation budget of the measurement device, the influence of deficits in the longwave radiation balance during night is assumed to be rather small (Mauder et al., 2008). However, effective radiation shielding does not only depend on the use of highly reflective materials but should also account for potential errors arising from interrupted convection processes within the shield through active ventilation (Lin et al., 2001). Yet, additional aspiration of the radiation shield depends on external power sources, and the cost of commercially available radiation shields often exceed those of the sensor itself (Young et al., 2014). The design and evaluation of inexpensive, passively ventilated radiation shields that combine effectiveness and reproducibility is therefore of great value for air temperature assessments in various research fields (Tarara and Hoheisel, 2007).

Here, we explored the performance of a low-cost measurement setup for air temperatures within the urban canopy layer. Using devices composed of an inexpensive temperature logger and a custom-made radiation shield for overall $62 USD, we developed a network of 79 measurement sites in and around the city of Bern (Switzerland) that has been operated during record-dry summer 2018. The first goal of this study was to assess data quality and potential sources of measurement errors of the passively ventilated low-cost devices (LCDs) by directly comparing them to actively ventilated automated weather stations (AWS) in three differing environments with regard to their degree of urban metabolism. By intercomparing UHI intensities retrieved by AWS and corresponding LCD measurements as well as by analysing the spatiotemporal variability of UHI magnitudes captured by the entire LCD measurement network across the built-up area, our second research aim was to evaluate the performance of the low-cost network in capturing intra-urban air temperature variability. Besides analyses over the entire study period (May 16th to September 15th 2018), we also examined an intense 9-days heatwave (July 30th to August 7th 2018) in order to assess the applicability of the LCD measurement approach under conditions with considerable thermal stress. After a critical discussion of our results, future challenges and potentials of low-cost measurement approaches for near-surface air temperatures in urban environments are outlined.

2. Materials and methods

2.1. Study area and climatology

The city of Bern is located in the western part of Switzerland at the boundary between the pre-alpine hills and the Swiss plateau. The main built-up area is shared by three municipalities (Bern, Köniz, Ostermundigen) with a total of 192′850 inhabitants (FINBE, 2018).

From north to south and west to east, the urban area covers about 10 by 11 km, respectively (Fig. 1a). Situated along the Aare River, the wider region of Bern is characterized by a complex topography stretching from 480.5 to 947.1 m a.s.l. (Fig. 1b).

Overall, Bern's climate is considered as temperate with an annual mean temperature of 8.8 °C and an average annual precipitation of 1059 mm for the reference period of 1981 to 2010 (MeteoSwiss, 2017). During summer months (June – August), average maximum temperatures vary between 21.6 °C (June) and 24.3 °C (July), whereas the mean number of heat days ($T_{max} > 30$ °C) is highest in July (2.9 days) and August (2.1 days). Due to dominant summertime convective precipitation, the period between May and September is the wettest throughout the year with mean monthly precipitation exceeding 100 mm. Local-scale topography is continuously interacting with meso-scale wind systems resulting from gradients between the mountains and the lowlands, whereas during calm synoptic situations, nocturnal slope winds advect colder air masses from the Alps (Wanner and Hertig, 1984).

The summer 2018 was marked by persistent high-pressure patterns over Northern and Central Europe (MeteoSwiss, 2018). The exceptional atmospheric patterns and resulting heat and dry extremes of this summer across the Northern Hemisphere were recently found to be linked to anthropogenic climate change (Vogel et al., 2019). In Switzerland, nationwide average temperature of the summer half-year (April – September) was the highest so far measured since 1864 and only 60% of mean precipitation was registered compared to the climatological norm period (1981–2010). An intense 9-days heatwave that took place north of the Alps from July 30th until August 7th with daily maximum temperatures above 30 °C (MeteoSwiss, 2018) was used to analyse the LCD measurement approach as well as spatiotemporal UHI patterns of Bern under extreme synoptic conditions.

2.2. Low-cost temperature measurement set-up

From May 16th to September 15th 2018 we assessed fine-scale spatiotemporal air temperature variability across the city and its surroundings using 79 thermistor-based HOBO Pendant® temperature loggers. After evaluating several small-sized temperature loggers under laboratory conditions, the main advantages for the choice of this logger were found to be its robustness, water-proof design, low battery use, and moderate unit price of $48 USD. Manufacturer-reported accuracy of less than ±0.5 K (within the temperature range of 0 to 40 °C) and resolution of 0.14 K (Onset, 2013) are comparable or better than those of temperature loggers in the similar price range (Hubbart et al., 2005; Gubler et al., 2018). The main drawback of this data logger is the relatively long *e*-folding time (or time constant) of 10 min for changes in ambient air temperatures due to the plastic (propylene) coating of the sensor (Table 1). However, with regard to the sampling rate of 10 min and subsequent hourly averaging of the instantaneous measurements, the effect of time lag induced biases was sought to be reduced. The storage capacity of 6′500 readings allowed for 43.5 consecutive days of data collection at the chosen interval. Reading out the data was done manually using an USB-interface every 30 to 40 days throughout the study period of 123 days. During these regular maintenance visits at each site, data were stored, sensor performance and its fixing were checked, shielding was cleaned, and metadata were updated.

In order to effectively shield the sensors from solar irradiance, we developed a radiation shield composed of five highly reflective, white 13 × 13 cm plates made of melamine formaldehyde resin (Fig. 2). We adopted a multi-plate design that has been shown to be the most effective for environmental purposes (Tarara and Hoheisel, 2007). Furthermore, a similar radiation shielding was successfully used in a previous study (Gubler et al., 2018), albeit with a different sensor and in a different environment. The plates are held together by three metal threaded bars, while white plastic spacers of 2 cm between each plate ensure equal spacing. The temperature logger is fixed onto the lowest plate which caused the sensor to be centred at the level of the second-highest plate. Although radiation shields formed of several reflective and UV-resistant plastic plates effectively shield solar radiation (Young et al., 2014), aspiration of radiation shields is recommended at urban sites due to hindered air circulation within the shield (WMO, 2006). However, as availability of external power sources needed for ventilation is often limited or not available in lower price segments (e.g., solar panel) we used a passively ventilated design potentially allowing for circulation of ambient air between the plates. The costs for one radiation shield were at $14 USD, which together with the temperature logger sums up to $62 USD per LCD.

2.3. Network design and characteristics

Meteorological networks in urban areas may, depending on the purpose, greatly vary in terms of density and extent (Muller et al., 2013a, 2013b). The main purpose of this study was to create a high-resolution data set of spatiotemporal air temperature variability in the urban canopy layer that allows for detailed evaluation of other cost-effective approaches in urban environments such as fine-scale climate modelling, interpolations of crowd-sourced data, and mobile measurements. This required not only to cover a heterogeneous mosaic of local-scale urban microclimates (Oke et al., 2017), but also to take into account topographical features as well as maximizing spatial coverage and density across the city. In a multistep process, we first developed a local-specific land surface classification based

Table 1
Technical air temperature sensor details of the low-cost measurement devices and the automated weather stations.

Sensor type	Variable	Ventilation	Accuracy	Resolution	*e*-Folding time (time constant)	Manufacturer
HOBO Pendant 8 k	Air temperature	Passive	±0.53 K (0 to 50 °C)	0.14 K	10 min (airflow 2 m s^{-1})	Onset Computer, Bourne MA, USA
Thygan VTP6	Air temperature, rel. humidity	Active	±0.15 K (−20 to 50 °C)	0.1 K	5 s (airflow 4 m s^{-1})	Meteolabor, Wetzikon, Switzerland

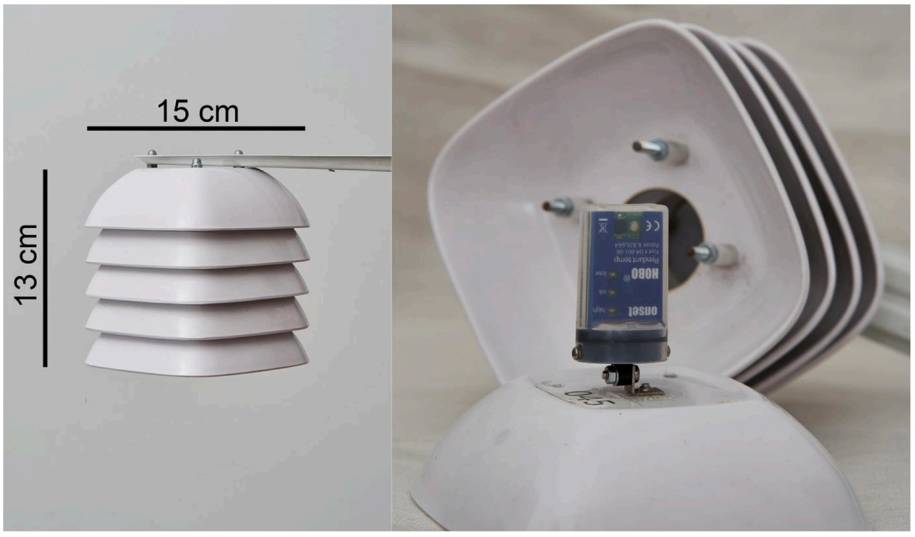

Fig. 2. Design and dimensions of LCD radiation shield and temperature logger (photo credits: P. Duschletta).

on the local climate zone (LCZ) framework (Stewart and Oke, 2012), available land cover data (EEA, 2012; AVR, 2015), information about building height (Swisstopo, 2017), and experts' knowledge (e.g., urban climatologists, architects, building physicists, and urban planners). On this basis, potential sites showing a directionally independent microclimate (ca. 100 × 100 m) that is representative for the local-scale land cover mix were selected and iteratively adjusted in discussion with experts and the city administration. Final locations were derived after an in-situ evaluation of representativeness as well as logistical considerations related to sensor mounting. Except for locations sought to represent a distinct microclimate (e.g., urban pocket parks), transitional zones between land use types were avoided where possible. To prevent attraction and damage through vandalism, sensors were installed between 2.67 and 3.20 m above ground, which is above standard height of 2 m but within the acceptable range for urban canopy layer temperature measurements (WMO, 2006). All devices were deployed to free-standing light posts, traffic lights, road signs, or power poles using white-painted metal angles of variable length depending on the pole diameter. We sought to minimize lateral heat sources by siting sensors away from large buildings, trees, and exhaust vents. However, due to restrictions in mounting options, a few observation sites were subject to a trade-off in that respect (e.g., Log_10 was deployed to a parking sign mounted on a building wall given the absence of poles in the middle of the street canyons within the historic centre; see supplementary material for detailed information).

The resulting network consisted of 73 measurement sites situated within the city (ca. 35 km^2) and six locations in the city's surroundings (ca. 110 km^2) representing rural reference sites that should also capture regional-scale weather dynamics (Fig. 1). Average spacing between sites was ca. 0.6 km (nearest neighbour), whereas the density of measurement sites decreased towards the city boundaries. The network represented a diversity of built environments (e.g., historic vs. modern, high/mid- vs. low-rise, industry vs. residential), land cover types (e.g., impervious surfaces, low vegetation, forest, agricultural lands, water bodies), topographical features (e.g., river channel, north vs. south-orientation), and points of public interest (e.g., main public transport station, public squares, city parks). In some cases, distance between two sites has intentionally been reduced to test for specific, local-scale temperature differences (e.g., park vs. concrete square, paved street vs. green avenue). The lowest site was at an elevation of 492.4 m a.s.l. and the highest site was situated at 656.7 m a.s.l., whereas average elevation was 547.5 m a.s.l. (SD = 24.5 m). Full metadata descriptions of each measurement site can be found in the supplementary material.

2.4. Data sources

2.4.1. Meteorological observations at reference sites

To test the effectiveness of the low-cost data loggers and the custom-made radiation shield, parallel measurements at three reference sites with automated weather stations (AWS) were conducted throughout the entire study period (Table 1). Although the reference sites differed in terms of distance to the city centre, prevailing land cover and local climatology (Fig. 1), air temperature was measured by the same type of actively ventilated, high-precision coupled thermo-hygrometer (Thygan VTP6; Meteolabor, 2019) at all three sites.

The first reference site (Zollikofen; hereafter ZOLL) was situated about 5 km north of the city centre in a rural environment (Fig. 1a) and is part of the automated observation network of the Swiss Federal Office of Meteorology and Climatology (MeteoSwiss), where the corresponding data was obtained from. Two LCDs were deployed at 2 and 3 m above ground (ZOLL_2m, ZOLL_3m) at a horizontal distance of about 6 m from the AWS. For the spatiotemporal UHI analyses, we used the ZOLL_3m as the rural reference, because this LCD was closer to the installation height of most sites of the urban network. In addition, we placed one data logger in a wooden Stevenson screen, a frequently used housing option for temperature sensors (van Meulen and Brandsma, 2008; Burton, 2014). This allowed for separate testing of the custom-made radiation shield against another passively ventilated shielding options and for

comparisons with previous studies (e.g., Young et al., 2014).

The second reference site (Wankdorf; hereafter AFU) was located in a suburban environment at about 2.5 km distance from the city centre (Fig. 1a) and is being maintained by the city's administration for protection of the environment and air quality. The site is located between a soccer stadium and a school building. Surrounding land cover consisted of a mix of grass patches, paved surfaces as well as single trees. The horizontal and vertical distance between the LCD and AWS was about 1.5 m and 0.3 m, respectively. Noteworthy, wind speed and direction were measured on the top of a building at a measurement height of 21.5 m above ground, which differs markedly from the wind measurement heights at the other two reference sites (10 and 40 m above ground).

The third reference site (Bollwerk; hereafter BOLL) is situated within the city centre just next to the main train station (Fig. 1a). Located on the roof of a multi-story building approximately 30 m above street level, the AWS is being maintained and corresponding data are distributed by the Federal Laboratories for Materials Testing (EMPA, 2018). The LCD was deployed at a horizontal and vertical distance of about 1 m and 0.5 m, respectively, from the AWS. Due to the location on the roof of the building, the site represents a distinct microclimate as it is decoupled from the canopy layer at street level, and, even though surrounded by buildings and impervious surfaces, the local horizon is unconstrained. Therefore, the site may not be directly compared to other LCDs at street level and has to be carefully interpreted. All meteorological variables were sampled at 10-min intervals and data sets for intercomparisons were made available by the responsible institutions.

2.4.2. Metadata

Detailed network and site descriptions as well as adequate communication of metadata are crucial but often missing in many UHI assessments and urban meteorological networks (Stewart, 2011; Muller et al., 2013a). Here, we collected a set of metadata at each site to ensure reproducibility and determination of potential site restrictions or measurement errors (see supplementary material). Whenever possible, metadata were assessed by direct measurements or observations during deployment or maintenance visits. This included information about location (e.g., coordinates, elevation), mounting (e.g., type, height, distance to pole), prevalent surface cover (e.g., photographs, general description), urban form (e.g., dimensions, building types) and urban function (land use), topographical features (e.g., depression, orientation), local horizon (e.g., hemispherical photographs), as well as general remarks regarding observed changes or potential error sources (e.g., construction work).

In addition, a set of variables relevant for local-scale climatology in urban environments (Stewart and Oke, 2012) such as surface cover fractions and sky view factor was retrieved from geospatial data being processed using the UMEP package (Lindberg et al., 2018) in QGIS 3.2.1 (QGIS Development Team, 2019). The underlying digital elevation model (swissALTI^{3D}) as well as building information (swissBUILDINGS3D 2.0) were obtained from the Federal Office of Topography (Swisstopo, 2017). Land cover data originated from the Office for Geoinformation of the Canton of Bern (AVR, 2015) and from the Urban Atlas land cover classification (EEA, 2012). Information about vegetation coverage, density, and height was based on high-resolution LIDAR data collected in 2012 (Ginzler and Hobi, 2015).

2.5. Data preparation and analysis

2.5.1. General data quality control

Prior to statistical analysis, a multi-step quality control was applied to account for potential artefacts in the data. First, temporal consistency with regard to potentially missing data was checked during manual compilation of the single data records from each site and measurement period into one data file based on date and time steps. Then, errors that arose during data collection visits due to sensor's exposure to direct sunlight when removing it from the radiation shield were identified. Thereby, the last data point before reading out the data records and the five subsequent data points were removed, resulting in a total of one hour (six data points) of missing data for each read-out. In a third step, metadata was consulted to identify and remove potentially erroneous data due to sensor demolishment, displacement, inadequate deployment, or significant changes of site characteristics that could bias measurements (e.g., temporary exhaust of warm air). Next, boxplots were analysed to locate measurements outside the range of physically plausible values. This plausible range was defined by maximum and minimum temperatures measured by any of the three AWS throughout the entire study period $\pm$5 K (plausible range: 0.7 to 39.2 °C). Data points outside this range were rigorously inspected and removed from the analyses. For the analyses presented here, quality control showed that only one data record (Log_22) exhibited physically implausible temperatures reaching up to 42.6 °C during the afternoon of August 5th. Consequently, the corresponding period was removed prior to the analysis (42 data points; 12:00–18:50 Central European Time; CET).

2.5.2. Intercomparison of LCD and AWS data

In order to evaluate the performance of the low-cost temperature logger and the custom-made radiation shield, we conducted statistical analyses on pairs of hourly averaged LCD and AWS temperature records at the three reference sites (ZOLL, AFU, BOLL). For each comparison, AWS data were subtracted from the LCD records, which in case of positive differences (ΔT) means that the LCD measured higher air temperatures than the AWS and vice versa for negative ΔT. Moreover, we calculated root-mean-squared errors (RMSE) between the LCD and the AWS for comparability with previous studies. Assessments of 2.5- and 97.5-percentiles allowed for the analysis of extreme values and statements about the range of ΔT for 95% of all data points.

Given that highest temperature differences between passively and actively ventilated radiation shields have been reported to occur during periods of high solar irradiance and low wind speeds (e.g., Tarara and Hoheisel, 2007; van Meulen and Brandsma, 2008; Burton, 2014), ΔT were analysed during day- and night-time separately. Night-time (daytime) values were extracted using a threshold of hourly averaged solar irradiance $\leq$1 W m^{-2} ($>$1 W m^{-2}) at ZOLL. The rural station was chosen due to the absence of artificial radiation

sources (e.g., street lightning) and the unrestricted horizon compared to the urban or suburban reference site. To assess contributions of solar irradiance and wind speed to potential daytime measurement biases, we calculated linear models based on a simplified correction modelling approach for unaspirated radiation shields developed by Auchmann and Brönnimann (2012). Given that potential biases due to radiative heating are theoretically highest at low wind speeds, an exponentially decreasing wind term accounts for this effect:

$$\Delta T = \beta 0 + \beta 1 \left(r \left(1 - exp\left(\frac{-k}{v} \right) \right) \right) \quad (1)$$

where ΔT is the temperature difference between the LCD and the AWS (in K), β_0 is the estimated intercept (in K), and β_1 denotes the estimated regression coefficient (K m^2 W^{-1}) of the predictor term expressed by r being the amount of solar irradiance (in W m^{-2}), v being the wind speed (in m s^{-1}), and k standing for the wind attenuation coefficient (in m s^{-1}). k was assigned a value of 2.6 m s^{-1} in order to fit the distribution of ΔT as suggested in Auchmann and Brönnimann (2012). Model performance was assessed by multiple R^2 as a measure of the amount of variance explained by the predictor term as well as by RMSE between modelled and measured ΔT, whereas the significance level of the predictors was $\alpha = p < 0.05$.

2.5.3. Evaluation of LCD measurement network

In addition to comparisons between LCDs and AWS over the entire study period, we assessed the performance of LCDs throughout the intense 9-days heatwave (July 30th until August 7th 2018) based on hourly averaged temperature data. The aim of this additional intercomparison between LCD and AWS measurements was to evaluate the ability of the LCDs to capture air temperature variability under extreme synoptic conditions. Although the analysis of raw biases between LCDs and AWS (ΔT) allows for inferences about potential implications of the bias regarding UHI intensity assessments, the extent to which the raw biases translate into UHI magnitudes may remain unclear. In order to be able to make quantitative statements about the performance of the LCD measurement network in capturing intra-urban air temperature variability, we also calculated hourly averages of UHI-based biases (ΔT_{UHI}) as the difference between UHI intensities derived from LCD temperatures and UHI intensities based on AWS data throughout the 9-days heatwave. Positive values of ΔT_{UHI} stand for overestimations of the UHI intensity by the LCDs, whereas in the case of negative ΔT_{UHI}, UHI intensities derived from LCD data are smaller and therefore underestimate the AWS UHI intensities. ΔT_{UHI} was calculated for both pairs of available rural vs. (sub-)urban reference sites, namely BOLL vs. ZOLL as well as AFU vs. ZOLL. These intercomparisons of UHI intensities retrieved by LCDs and AWS (ΔT_{UHI}), respectively, were then compared to the raw biases (ΔT) in order to assess the extent of over- or underestimation of the UHI magnitudes by the LCDs during day- and night-time. Moreover, the UHI bias assessment and its comparison with raw biases at the three reference sites was used as the basis for the (qualitative) discussion of site-specific factors that might have impacted the UHI intensity measurements by the LCDs at different sites of the measurement network.

In addition to the UHI bias assessment during the heatwave, the value added by the LCD measurement network compared to the three existing AWS for the analysis of intra-urban air temperature variability was on the one hand examined by comparisons of UHI variabilities over the entire study period between the LCD network sites and those retrieved from the two AWS located within the city (AFU, ZOLL). On the other hand, we used spatiotemporal assessments of UHI intensities during the 9-days heatwave to evaluate benefits and shortcomings of the fine-scaled LCD measurement network for assessments of intra-urban air temperature variability in a city with complex topography.

2.5.4. Assessment of UHI intensities

Given that the UHI is known to be most pronounced during night, UHI intensities over the entire study period were calculated for night-time only (solar irradiance at AWS ZOLL $\leq$1 W m^{-2}), whereas during the heatwave, full day UHI magnitudes were assessed. The canopy layer UHI intensity is defined as the difference between temperature observations in the city and its rural surroundings (Oke, 1982). However, regarding the multitude of small-scale variations in land cover and intra-urban effects influencing local temperatures across a city, the use of as few as two stations (urban vs. rural) is not appropriate (Stewart and Oke, 2012). A wide range of alternative approaches for more representative definitions of urban and rural sites have therefore been suggested: Averaging two or more stations with similar characteristics (Smoliak et al., 2015), site classifications based on single parameters such as fractions of impervious surface (Schatz and Kucharik, 2015), or classifying a site's local climate zone based on several physical parameters (Stewart and Oke,

Table 2
Mean values (ΔT_{avg}), ranges (ΔT_{range}), percentiles (ΔT_{perc}), and root mean square errors (RMSE) of hourly averaged temperature differences [K] between LCDs and AWS at the three reference sites throughout the entire study period (May 16th to September 15th 2018). Beside overall differences (full day), daytime and night-time differences are shown separately.

	Overall ΔT_{avg} (K)	Overall ΔT_{range} (K)	Overall ΔT_{perc} 2.5%; 97.5% (K)	Overall RMSE (K)	Daytime ΔT_{avg} (K)	Daytime ΔT_{range} (K)	Daytime ΔT_{perc} 2.5%; 97.5% (K)	Day-time RMSE (K)	Night-time ΔT_{avg} (K)	Night-time ΔT_{range} (K)	Night-time ΔT_{perc} 2.5%; 97.5% (K)	Night-time RMSE (K)
ZOLL _3m	0.55	−0.57; 2.7	−0.13; 1.57	0.71	0.71	−0.57; 2.7	−0.04; 1.67	0.85	0.23	−0.42; 1.27	−0.17; 0.85	0.34
ZOLL _2m	0.5	−0.92; 2.48	−0.28; 1.6	0.78	0.78	−0.77; 2.48	−0.08; 1.7	0.95	−0.02	−0.92; 0.65	−0.38; 0.28	0.21
AFU	0.56	−0.68; 2.53	−0.38; 2.03	0.95	0.93	−0.5; 2.53	−0.23; 2.12	1.17	−0.12	−0.68; 0.27	−0.45; 0.13	0.2
BOLL	0.4	−1.02; 2.66	−0.3; 1.53	0.64	0.61	−1.02; 2.66	−0.17; 1.65	0.78	0.02	−0.63; 0.48	−0.37; 0.32	0.19

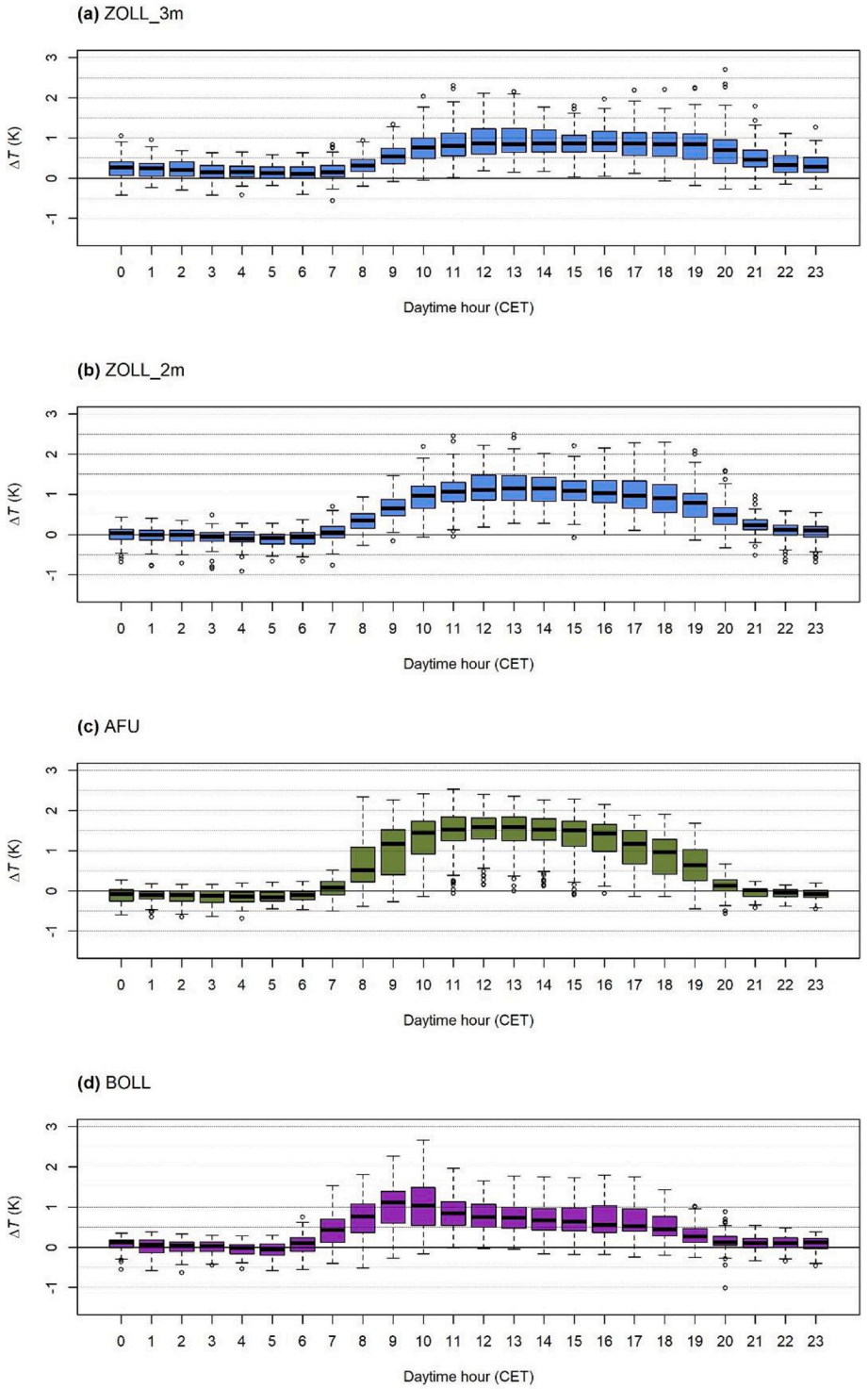

Fig. 3. Boxplots of hourly averaged temperature differences ΔT (K) throughout the entire study period (May 16th to September 15th 2018) between LCDs and AWS split by daytime hours (CET). Differences are shown for the LCD deployed at a) 3 m and b) 2 m above ground at site ZOLL, as well as at the sites c) AFU and d) BOLL.

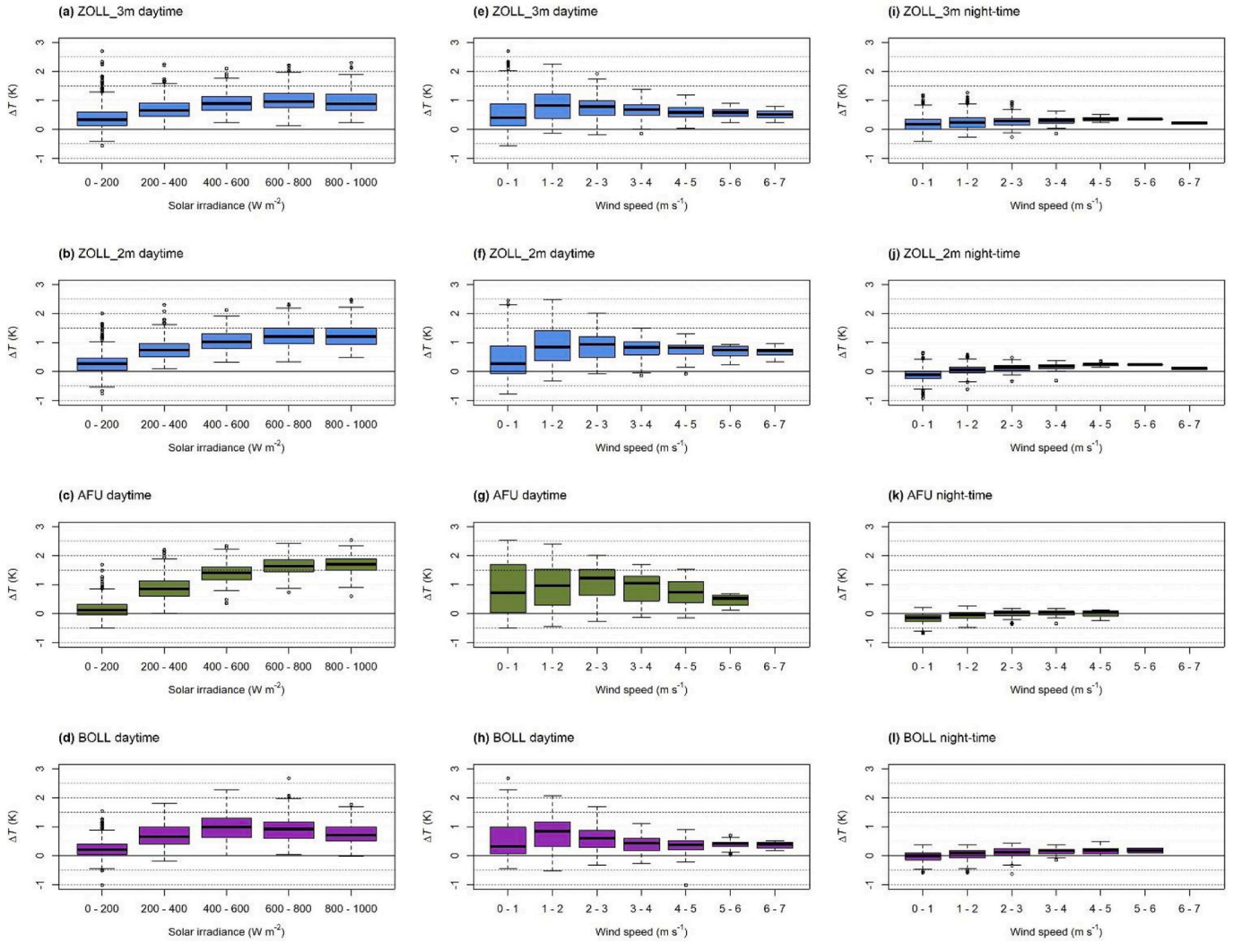

Fig. 4. Boxplots of hourly averaged temperature differences ΔT (K) grouped by levels of solar irradiance and wind speed during daytime (a – h) and night-time (i – l) over the entire study period (May 16th to September 15th 2018). Differences are shown for the LCDs deployed at 3 m (a, e, i) and 2 m (b, f, j) above ground at site ZOLL, as well as at the sites AFU (c, g, k) and BOLL (d, h, l).

2012).

For this case study, we refer on the one hand to the traditional UHI definition and use the WMO-certified site ZOLL as rural reference station. By subtracting its LCD temperature record from those of all other observation sites, we explored spatial patterns of UHI intensity in detail. Except for differences in absolute temperature, UHI intensity also manifests in distinct cooling rates of the urban canopy layer. Due to rural sites being generally more open to the sky, rural cooling rates during the evening are generally higher than in urban environments due to open horizon and generally lower thermal admittance of surface materials. Conversely, urban sites' horizon is often restricted (e.g., in street canyons) and thermal admittance of materials is high (Oke et al., 2017). For each measurement site, we therefore also calculated cooling rates ($-\Delta T/\Delta t$) as the difference of hourly mean temperatures at 18:00 and 22:00 CET. This time interval was chosen due to the cooling gradients of near-surface air masses, at least in mid-latitudes, are assumed to be largest between late afternoon and early night-time (Oke et al., 2017).

Data of three LCD measurement sites was not taken into account for the analysis of UHI intensities and cooling rates, either due to missing data during more than four subsequent hours (Log_14, Log_27) or the fact that the site was primarily used for reference measurements (Log_64) and therefore had been installed in a non-comparable setting (e.g., rooftop). As a consequence, data from a total 76 measurement sites was used for the UHI analysis over the entire study period as well as during the heatwave.

Despite the relatively complex topography of the study area and resulting elevation variations across the measurement sites (Fig. 1), we did not correct for potential effects of elevation differences on the temperature data such as by removing the background air mass' lapse rate. Although a height correction would allow for more detailed analyses of thermo-dynamical processes (e.g., cold air pooling) and is generally recommended for UHI studies (Stewart, 2011), the intention of this study was to precisely assess absolute air temperatures relevant for human comfort, which would be less realistic on the basis of potential temperatures resulting from elevation correction.

Whereas all statistical analyses and corresponding illustrations were conducted using the software R x64 4.0.2 (R Core Team, 2019), spatial patterns were investigated using maps created in ArcGIS Pro 2.4.0 (Esri, 2019).

3. Results

3.1. Evaluation of low-cost measurement equipment

3.1.1. Performance of LCDs over the entire study period

In order to evaluate performance of the low-cost measurement setup, we compared mean differences (ΔT) and root-mean-square errors (RMSE) between the hourly averaged LCD and AWS records at the three reference sites. Over the entire study period, the comparison between LCDs and AWS (Table 2) reveals positive biases with mean ΔT between 0.4 K and 0.56 K and RMSEs ranging from 0.64 K to 0.95 K. Mean values of ΔT as well as RMSEs are lowest at the urban reference site BOLL, whereas highest biases occur at the suburban site AFU. During daytime, differences between the LCD and AWS are highest and result in diurnal averages of ΔT between 0.63 and 0.93 K and RMSEs ranging from 0.78 K to 1.17 K. Hourly averaged ΔT during daytime overall varies between −1.02 and 2.7 K, whereas the analysis of 97.5-percentiles shows that ΔT larger than 2.12 K can be considered as outliers. Taking into account the 2.5-percentiles, more than 95% of hourly averaged daytime LCD temperatures differ between −0.38 and 2.12 K from the AWS. In accordance with overall averages of ΔT and RMSE, daytime biases are highest at the suburban site AFU and lowest at the urban site BOLL. During night, differences between the LCDs and AWS are substantially smaller across all reference sites. Mean nocturnal ΔT varies between −0.12 and 0.23 K with corresponding RMSEs between 0.19 K and 0.34 K. Hourly averages of ΔT during night-time range within a range of −0.92 to 1.27 K. Analyses of extreme percentiles suggest that more than 95% of all nocturnal hourly averages of LCD measurements are subject to differences between −0.45 and 0.85 K compared to the AWS data. Unlike biases during daytime, highest mean nocturnal ΔT and RMSEs occur at ZOLL_3m, whereas lowest differences are found at the urban site BOLL as well as ZOLL_2m. At the suburban site AFU and at ZOLL_2m, mean night-time ΔT is slightly negative.

Splitting ΔT by hours of the day (CET) generally reveals similar diurnal patterns at the three reference sites (Fig. 3). During night-time (hours 22 to 6), ΔT is lowest with median values varying from −0.17 to 0.33 K and relatively small variability at all sites. Predominantly at ZOLL_2m, BOLL, and AFU (Fig. 3b-d), median differences between LCDs and AWS turn eventually negative during night, indicating that LCDs measure lower temperatures than the AWS. Subsequent to sunrise (hours 7 to 12), median values as well as the ranges of ΔT increase rapidly at all sites. However, gradients of ΔT during the morning differ across the sites with markedly stronger increases at the site AFU (Fig. 3c) compared to ZOLL and BOLL (Fig. 3a-b, d). Notably, medians and extreme values of ΔT at BOLL (Fig. 3d) peak during the hours 9 and 10, a pattern that is not observed at the other two sites. Throughout the afternoon (hours 13 to 17), differences between LCDs and AWS remain elevated at all sites implying LCD being predominantly higher than AWS temperatures. Moreover, afternoon median and maximum values of ΔT at suburban site AFU (Fig. 3c) distinctly exceed those of the two other sites. During the evening (hours 18 to 21), median and range of ΔT decrease at all sites. However, these declines are strongest at ZOLL_2m, AFU and BOLL (Fig. 3b-d), whereas at compared to ZOLL (Fig. 3a) the decrease is less pronounced and appears to be lagged by a few hours.

3.1.2. Bias source evaluation over the entire study period

The above finding of relatively higher ΔT and RMSE between LCDs and AWS occurring during daytime compared to night-time suggests solar radiation as a likely source of the bias. Comparisons of boxplots of hourly averaged diurnal ΔT grouped by levels of solar irradiance at each reference site (Fig. 4a-d) indeed imply a positive correlation between observed temperature differences and the amount of solar irradiance. As such, higher medians of differences between LCD and AWS temperatures generally coincide with higher

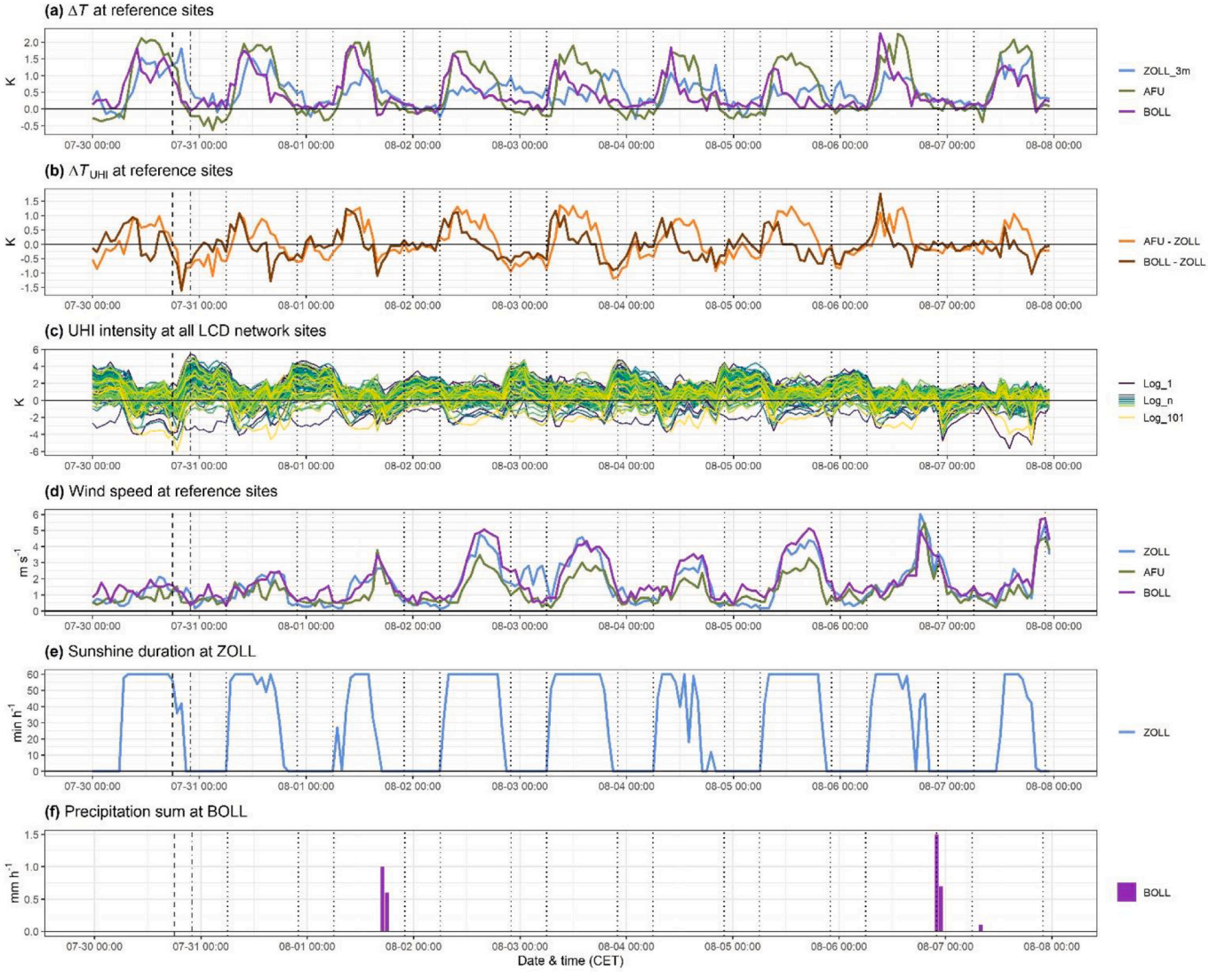

Fig. 5. Temporal variability of hourly averaged a) ΔT (K) at the three reference sites (ZOLL, AFU, and BOLL) and b) ΔT_{UHI} (K) between two pairs of reference sites (AFU-ZOLL and BOLL-ZOLL) during the intense heatwave between July 30th and August 7th 2018. Furthermore, c) UHI intensity (K) at all LCD sites of the measurement network, d) wind speed (m s^{-1}) at all three reference sites, as well as e) sunshine duration (min h^{-1}) at ZOLL and f) hourly precipitation sum at BOLL (mm h^{-1}) are shown. Vertical dashed lines indicate the periods used for the analysis of spatial UHI patterns (July 30th 22:00 CET) and cooling rates (July 30th 18:00–22:00 CET; see Fig. 6). Vertical dotted lines refer to the separation between night-time (22:00–06:00 CET) and daytime (06:00–22:00 CET).

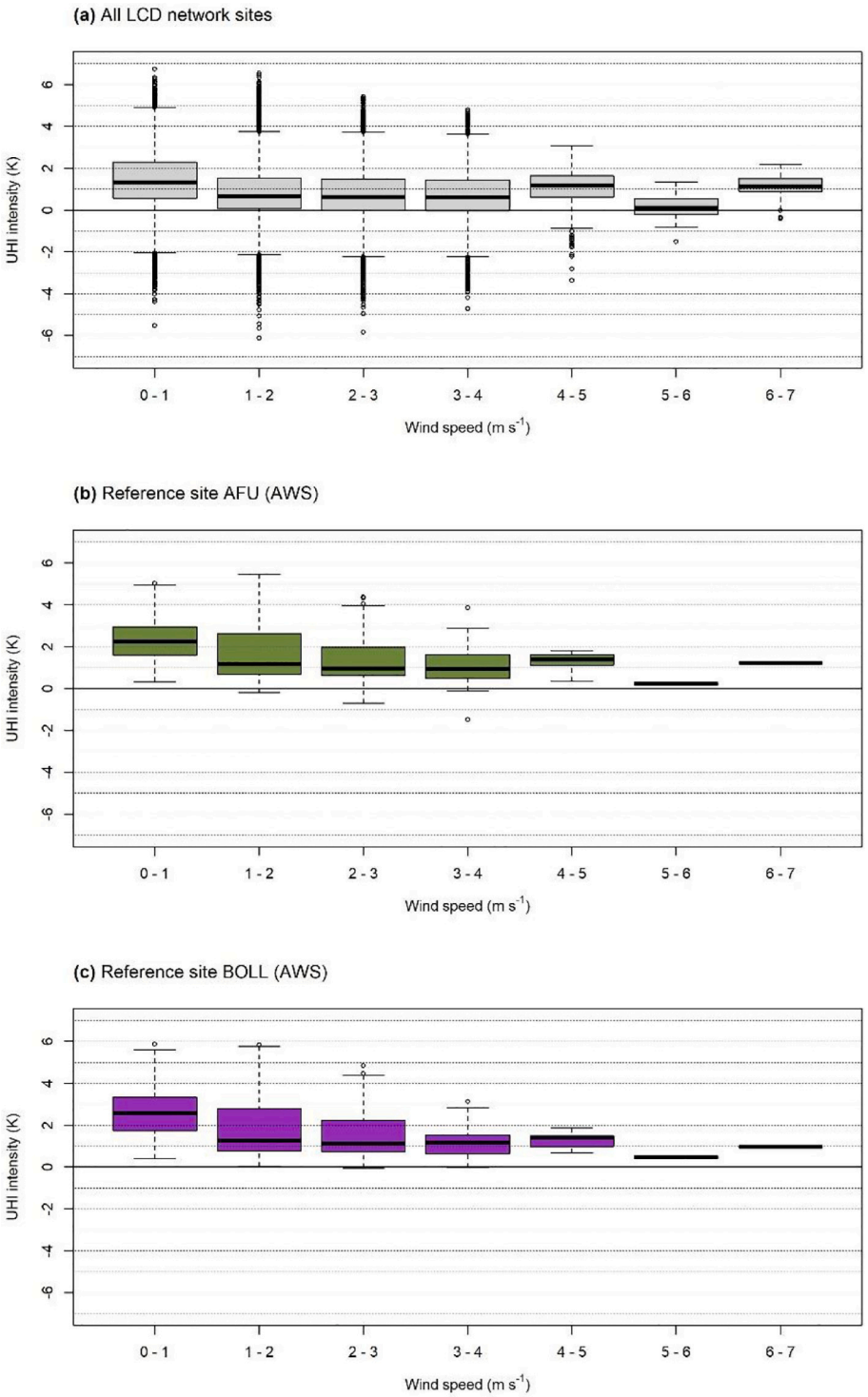

Fig. 6. Boxplots of hourly averaged night-time UHI intensities (K) over the entire study period (May 16th to September 15th 2018) and grouped by levels of wind speed retrieved from rural AWS ZOLL). UHI intensities are shown a) for all sites of the LCD measurement network, b) for the suburban AWS AFU, and c) for the urban AWS BOLL.

levels of solar irradiance. Conversely, medians of ΔT are in general lower during conditions of reduced solar irradiance. This relationship is most clearly pronounced at the site AFU (Fig. 4c) with median biases above 1 K as well as high values of ΔT (>2 K) predominately co-occurring with enhanced levels of solar irradiance (>400 W m^{-2}). At ZOLL_3m and ZOLL_2m (Fig. 4a-b), high values of ΔT (>2 K) are also registered in situations with only small amounts of solar irradiance (<200 W m^{-2}), and medians of ΔT level off (ZOLL_2m; Fig. 4b) or even slightly decrease (ZOLL_3m; Fig. 4a) at highest solar irradiance (>800 W m^{-2}). The pattern of BOLL (Fig. 4d) reveals a peak with the highest median of ΔT occurring between 400 and 600 W m^{-2}, whereafter the medians of ΔT decrease for conditions of higher solar irradiance (>600 W m^{-2}). Notably, one distinct negative outlier (<1 K) is observed at very low levels of solar irradiance (<200 W m^{-2}).

Radiative biases predominantly occur in case of limited mixing causing accumulations of heat inside the radiation shield. Due to the multi-plate design of the LCD shielding and the absence of additional aspiration, natural ventilation by prevailing winds is likely to be reduced. As expected, highest values of ΔT (>2 K) coincide with low wind speeds (<2 m s^{-1}) during the day at all three sites (Fig. 4e-h). Whereas the variances of ΔT at all sites gradually decrease in response to higher wind speeds, medians of ΔT are lowest at either very low (0 to 1 m s^{-1}; ZOLL and BOLL) or very high wind speeds (5 to 6 m s^{-1}; AFU) and peak at wind velocities between 1 and 3 m s^{-1} at all sites. This pattern is similarly found across all sites with only one exception relating to the negative outlier at BOLL (Fig. 4h), which occurs at relatively high wind speeds of 4 m s^{-1}. In sum, the patterns of reduced variance as well as decreasing maximum values and medians of ΔT in response to higher wind speeds support the reasoning of natural ventilation by prevailing winds playing an important role for measurement biases of the LCDs.

Linear regression models testing the combination of solar irradiance and wind speed as main sources of daytime ΔT reveal varying results (Table S1). Model performance is best at the suburban site AFU with more than 82% of the variance in ΔT explained by solar irradiance and wind speed (adjusted R^2: 0.828). At BOLL and ZOLL_2m, model performance is of similar magnitude with 54% and 64% of explained variance (adjusted R^2: 0.54 and 0.647). Regarding the LCD deployed at 3 m above ground at the rural site ZOLL, model performance is considerably lower with 38% of the variance explained (adjusted R^2: 0.385).

During nocturnal absence of solar irradiance, variances of ΔT are generally reduced with increasing wind speeds at all sites (Fig. 4i-l). Depending on the site, the signs of the median ΔT are predominantly positive (ZOLL_3m, Fig. 4i; BOLL, Fig. 4l) or mixed (ZOLL_2m, Fig. 4j; AFU, Fig. 4k). Highest overall variabilities of ΔT are found at the rural sites ZOLL_3m and ZOLL_2m (Fig. 4i-j) with ΔT varying from −0.42 to 1.27 K and − 0.92 to 0.65 K, respectively. Although wind speeds higher than 5 m s^{-1} only rarely occurred during night-time, the nocturnal patterns of ΔT indicate a buffering effect of prevailing winds on LCD biases by increased ventilation of the radiation shield.

Comparisons between LCD and a temperature logger housed in a wooden Stevenson screen at site ZOLL (not shown here; see Fig. S1) show daytime ΔT ranging from −1.28 to 1.28 K and predominately positive medians. In alignment with findings from comparisons with the AWS (Fig. 4), medians and maximum values ΔT increase in response to higher amounts of solar irradiance (Fig. S1a). Similarly, the variance of daytime biases is reduced at higher wind speeds (Fig. S1b). Night-time differences are predominately negative and range from −0.98 to 0.05 K (Fig. S1c). In sum, ΔT between LCD and the Stevenson screen is markedly smaller than when compared to the AWS. Moreover, daytime differences between LCD fixed at 3 m and LCD fixed at 2 m above ground at site ZOLL are overall small (range: −0.72 to 1.12 K), and medians of ΔT turn negative as a function of higher solar irradiance (Fig. S1d). A similar pattern is observed at increasing wind speeds (Fig. S1e), whereas variances of ΔT are also decreasing at higher wind speeds. During night-time (Fig. S1f), ΔT is predominately positive (range: −0.05 to 1.0 K) and medians as well as variances decrease in response to higher wind speeds, altogether indicating that differences in measurement height may be of relevance at rural site ZOLL.

3.1.3. *Performance of LCDs during heatwave*

From July 30th until August 7th 2018, the city of Bern was hit by an intense heatwave with daily maximum temperatures over 30 °C during a period of 9 consecutive days. In accordance with the findings of the evaluation across the entire study period, hourly averaged ΔT at the reference sites vary between −0.6 and 2.2 K throughout the heatwave (Fig. 5a) with highest values occurring during afternoon hours. This may be attributed to radiative heating and limited ventilation of the radiation shield due to reduced wind speeds (<1–2 m s^{-1}; Fig. 5d) at that time of the day. On the other hand, lowest values are registered after sunset, in the absence of pronounced wind velocities, during daytime periods of reduced sunshine (Fig. 5e), and in co-occurrence with precipitation events (Fig. 5f). Although daily variations of ΔT appear to be similar at all three reference sites, daytime ΔT at suburban site AFU are up to 0.5 K higher than those at the other two sites. In line with the findings across the entire study period, this could be explained by generally lower wind speeds recorded at this AWS during daytime leading to poor ventilation of the radiation shield (Fig. S2b). In addition, the decrease in ΔT after sunset at rural site ZOLL appears to be lagged and results in relatively higher (up to 1 K on August 5th) nocturnal biases than at the two other sites. Comparison with prevailing winds shows that this lag predominantly occurs in situations with reduced wind speeds (<2 m s^{-1}). Inter-site differences with diurnal maxima of ΔT are generally highest at site AFU and lowest at site ZOLL (Fig. 5a) and indicate a potential contribution of site-specific factors on LCD air temperature records. This is further strengthened by noticeable decreases of ΔT at the site BOLL during early afternoons coinciding with elevated wind speeds (Fig. 5d).

Comparisons of UHI intensities (ΔT_{UHI}) derived from LCD and AWS data (Fig. 5b) reveal differences varying between −1.6 and 1.8 K, whereas during daytime, ΔT_{UHI} is predominately positive and subject to marked variability (range: −1.6 to 1.8 K). Largely in line with positive ΔT at the reference sites (Fig. 5a), the general overestimation of UHI intensities by the LCDs during daytime is likely linked to radiative heating and poor ventilation of the LCD radiation shield. However, daytime ΔT_{UHI} also show distinct patterns depending on the pair of reference sites considered (Fig. 5b). As such, ΔT_{UHI} derived from BOLL vs. ZOLL regularly decrease and eventually turn negative around noon or during early afternoon, whereas ΔT_{UHI} from AFU vs. ZOLL remain positive throughout the afternoon hours. This might be attributed to differences in wind speed between the urban (BOLL) and suburban (AFU) reference sites.

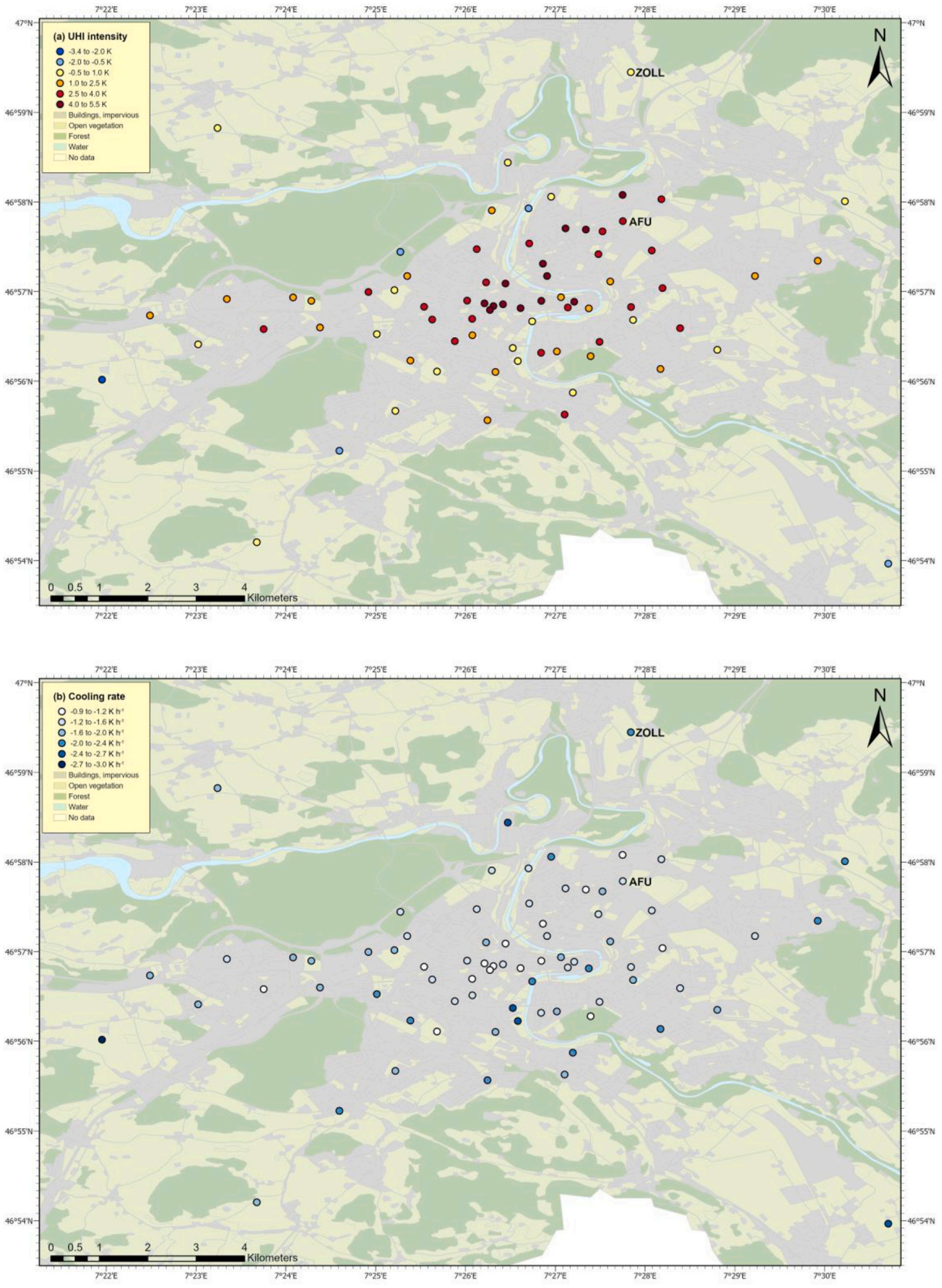

(caption on next page)

Fig. 7. Spatial variability of UHI characteristics during late afternoon and early night of July 30th across the LCD measurement network and different land cover types (Urban Atlas; EEA, 2012). UHI intensity a) denotes differences of hourly average temperatures (K) at 22:00 CET between LCD at rural site ZOLL and all other LCD sites (local time; CEST), whereas cooling rates b) are defined by mean differences between hourly averaged air temperatures at 18:00 and 22:00 CET (Kh^{-1}) at all sites. Map coordinates refer to the World Geodetic System 1984 (WGS84), which was used for the map projection in ArcGIS Pro 2.4.0 (Esri, 2019).

Wind speed is markedly higher at BOLL during noon and afternoon hours than at AFU (Fig. 5d). Abrupt minima of negative ΔT_{UHI} observable for both pairs of sites during afternoon and early evening hours seem to be either the product of sudden changes in meteorological conditions (Fig. 5d-f; e.g., solar irradiance on July 30th, or precipitation and wind on August 1st) or to be related to site-specific local-scale factors influencing the rural site ZOLL (e.g., on August 3rd), whose temperature records were used for the calculation of both pairs. During night-time, variability of ΔT_{UHI} is markedly lower (range: −1.1 to 0.4 K) and predominately negative, which indicates an underestimation of the UHI intensity by the LCD measurements. This pattern likely reflects reduced ΔT in absence of solar irradiance (Fig. 5a), although negative ΔT_{UHI} being more pronounced for the pair AFU vs. BOLL also points towards differences in site-specific characteristics.

3.2. Application of LCD measurement network for UHI assessment

3.2.1. UHI variability over the entire study period

To explore the applicability and performance of the LCD measurement network, we calculated and compared nocturnal UHI intensities over the entire study period between the two urban-rural pairs of AWS (AFU vs. ZOLL and BOLL vs. ZOLL) as well as between the LCD at the rural reference site ZOLL_3m and all other LCD sites (Fig. 6). UHI intensities from the LCD measurement network (Fig. 6a) range between −6.13 and 6.74 K with the highest median and maximum UHI intensities being recorded during conditions with very low wind speed (0 to 1 m s^{-1}). Variance is found to be highest with low wind (1 to 2 m s^{-1}) and generally decreases with increasing wind speed, which very likely reflects the effect of advection and stronger atmospheric turbulence that lowers intra-urban air temperature variability. UHI intensities recorded by the suburban AWS AFU (Fig. 6b) and by urban AWS BOLL (Fig. 6c) vary from −1.5 to 5.47 K and − 0.5 to 5.87 K, respectively. Following from this, UHI intensities assessed at the two AWS show a markedly lower variability than those retrieved from the LCD measurement network, which holds particularly true for negative UHI magnitudes, a situation very rarely recorded at the two AWS. In accordance with the LCD pattern, however, median UHI intensities from the AWS are highest with low wind speeds (0 to 1 m s^{-1}) and maximum UHI variances are recorded at wind speeds of 1 to 2 m s^{-1}. It should be noted that the condition of high wind speeds (5 to 7 m s^{-1}) occurred only once, and the meaningfulness of comparisons between LCD and AWS UHI intensities is thus limited due to incomplete boxplots.

3.2.2. UHI variability during heatwave

In order to analyse the applicability of the LCD measurement network in a situation with considerable heat stress synoptically extreme situation, we assessed the spatiotemporal UHI variability during the intense 9-days heatwave (July 30th until August 7th 2018). Throughout this period, UHI intensities vary considerably (Fig. 5c) with maximum values up to 5.5 K typically occurring between sunset and midnight, as well as in the early morning before sunrise. During five out of eight investigated nights, UHI intensities of 4 K or more are being recorded at 17 LCD sites. Regarding the meteorological parameters measured at the three AWS, these elevated nocturnal UHI intensities may be interpreted as a consequence of high amounts of solar irradiance during the previous day (Fig. 5e) and low wind speeds at night (Fig. 5d). Conversely, night-time UHI magnitudes are less pronounced after days with limited sunshine or prevailing winds. Negative UHI intensities, implying lower temperatures at the corresponding LCD sites compared to the rural reference site, are generally more pronounced during afternoons and early nights. The heatwaves' minimum UHI intensity of −5.9 K is registered around sunset of July 30th, whereas highly negative UHI magnitudes generally tend to co-occur with changes in meteorological conditions such as enhanced variability of wind speed or solar irradiance recorded at the AWS.

To assess spatial characteristics of Bern's UHI during the heatwave, we focussed on the UHI intensity at 22:00 CET on July 30th (Fig. 7). High UHI intensities of 4 to 5.5 K are mainly recorded in densely built-up areas of downtown districts (LCZ 2) as well as within adjacent residential areas (LCZ 5 and 6; Fig. 7a). Although UHI intensity is generally moderate (1 to 2.5 K) in suburban areas with higher portions of vegetated surfaces, this pattern is not consistent with regard to several locations in the eastern and southern parts of the city showing distinctly higher values of the UHI between 2.5 and 4 K. Except for one site being located in a residential area, these measurement locations are situated in industrial and commercial districts as well as adjacent to highways. On the other hand, relatively less pronounced UHI magnitudes are also found to occur at sites close to the city centre. As a result, steep gradients of UHI intensity occur within relatively short distances of several 100 m. Moderately positive and negative UHI intensities (−2.5 to 1 K) are mostly restricted to open spaces with low vegetation (e.g., parks, allotment gardens, cemetery) and forests. Similar negative UHI intensities are observed at sites along the river channel crossing the city, which are characterized by the lowest elevations of the study area and are thus prone to rapid cold air accumulations. Minimum UHI intensity (−3.4 K) is registered at the most western site being situated in a local topographic depression. Due to ΔT_{UHI} of about 0.5 K being found at 22:00 between LCD and AWS at ZOLL (see Fig. 5b), resulting UHI intensities might even be slightly higher for many sites as the LCD-based UHI intensity is underestimated.

In addition to the analysis of hourly averaged maximum UHI intensity after sunset (22:00), mean hourly cooling rates ($-\Delta T/\Delta t$) from late afternoon to early night (18:00–22:00 CET) were calculated (Fig. 7b). Hourly cooling rates overall range from −0.9 to −3 K

h^{-1} with a tendency for stronger cooling towards the outer parts of the city. Highest cooling rates (−2.4 to −3 K h^{-1}) are being observed at five sites, of which one is situated in the above mentioned local topographic depression and four in the river valley. On the other hand, moderate cooling (−1.6 to −2.4 K h^{-1}) occurs mostly at rural sites, in suburban areas, residential or recreational sites with high portions of vegetation, and along the river channel. Low cooling rates (−0.9 to −1.6 K h^{-1}) are particularly found within the city centre, in densely built-up residential areas, across commercial and industrial districts, and at forested sites. However, some sites in the outlying districts east and west of the city centre are also subject to low cooling rates. Thus, patterns of cooling rates seem to be characterized by pronounced inter-site heterogeneity depending on fractions of vegetated surfaces and of built-up areas. In addition, topography likely also contributes to cooling variability as sites along the river channel, and some of the rural sites in the western parts of the study area differ markedly from neighbouring sites.

With regard to the UHI characteristics at the LCD located at the two AWS sites (ZOLL, AFU) used in the UHI analysis, it can be noted that the UHI intensities (Fig. 7a) as well as cooling rates (Fig. 7b) being recorded there are on the one hand representative for comparable settings in terms of topography and land cover. On the other hand, the two AWS locations only represent a small fraction of the UHI characteristics captured by the entire LCD network, in particular with regard to densely built-up areas and topography.

4. Discussion

4.1. Performance of LCDs

Intercomparisons between LCDs and AWS over the entire study period revealed positive mean biases at all three reference sites (Table 2), whereas ΔT was substantially larger during daytime compared to night-time (Fig. 3a-d). With regard to maximum daytime ΔT, several studies reported a bias >2 K (Hubbart et al., 2005; Nakamura and Mahrt, 2005; Young et al., 2014; Bell et al., 2015), which is within a similar range as our finding of extreme biases up to 2.7 K. However, these extreme biases did not occur systematically and may be a result of short-term disturbances. Observed mean diurnal ΔT of 0.61 to 0.93 K throughout the entire study period exceed former findings of 0.2 to 0.3 K (Richardson et al., 1999), 0.39 K (Nakamura and Mahrt, 2005), 0.42 K (Mauder et al., 2008), or 0.1 K (Young et al., 2014). Only Bell et al. (2015) reported similar or even higher mean daytime biases (0.9 to 2.1 K) for some of the evaluated citizen weather stations. The mean biases of the LCDs were almost twice as high as the measurement accuracy of the sensor as stated by the manufacturer (0.53 K). Throughout the heatwave (Fig. 5a), hourly averaged ΔT usually peaked during daytime with daily maxima between 0.7 and 2.2 K depending on the reference site. Although the performance of the LCDs, at least during daytime, appeared to be lower compared to other low-cost shielding and sensor types, the sources of the resulting biases are well understood. Based the amount of solar irradiance and prevailing wind speed, ΔT could be considerably well modelled by linear regression models at all sites (Table S1) with remaining residual standard errors (0.3 to 0.36 K) at similar magnitudes than previously presented lower cost sensors and radiation shields. Consequently, the here presented LCD measurement approach can be considered to capture diurnal air temperatures in urban environments at comparable accuracies given the availability of radiation and wind data that may be used for subsequent modelling and correction of the bias.

During night-time, when the emission of longwave radiation dominates the energy balance of the radiation shield, mean ΔT between LCDs and AWS over the entire study period were markedly lower with −0.12 to 0.23 K (Table 2; Fig. 3). Throughout the heatwave, nocturnal biases predominately varied between −0.5 and 0.5 K, with a few exceptions at the rural site ZOLL (Fig. 5a). These deviations correspond with nocturnal biases presented in previous studies (Anderson and Baumgartner, 1998; Nakamura and Mahrt, 2005; Mauder et al., 2008). Given that the observed mean ΔT were within the sensor-specific accuracy, we argue that our low-cost measurement equipment is suited for the evaluation of nocturnal air temperature variability in urban environments.

Comparability of measurement errors across existing intercomparison studies of LCDs is limited by the heterogeneity regarding reference sensor used, shielding type, measurement location, weather conditions, and length of the study period (Huwald et al., 2009). For instance, one of the few evaluations of low-cost sensors and radiation shields designed for the use in urban environments (Young et al., 2014) was based on comparisons with a reference sensor being housed in a Stevenson screen. Although having been used as standard radiation shielding by many meteorological services throughout the last century, this type of naturally ventilated radiation screen was shown to be similarly subject to significant measurement biases due to radiative heating and poor ventilation (van Meulen and Brandsma, 2008; Burton, 2014). In view of our finding of substantially smaller ΔT of LCD when compared to a Stevenson screen (Fig. S1a–c), this suggests that the relatively small temperature biases found by Young et al. (2014) would most probably be higher if compared to an actively ventilated reference sensor. As a consequence, biases of low-cost sensors and naturally ventilated radiation shields should be interpreted with caution depending on the specific contexts of the comparison and the intended field of application. To allow for meaningful comparisons of different shielding and sensor types, intercomparisons would therefore need to be conducted on a standardized basis with similar reference instruments (e.g., actively ventilated temperature sensor), during periods of comparable climatology (e.g., summer months), at similar reference sites (e.g., WMO-compliant weather stations), and at similar reference heights (e.g., 2 or 3 m above ground).

4.2. Sources of LCD biases

In line with results from existing studies examining the performance of Gill-like, naturally ventilated radiation shields (Hubbart et al., 2005; Nakamura and Mahrt, 2005; Tarara and Hoheisel, 2007; Mauder et al., 2008; Young et al., 2014), the combined effects of incident solar irradiance and low wind speed were found to be significant sources of LCDs biases during daytime hours (Fig. 4a-h; Table S1). Consequently, LCD performance during the day generally decreased in response to high solar irradiance and low wind

speeds. However, non-linearity of the observed patterns, distinct extreme biases of more than 2.5 K occurring at reduced amounts of solar irradiance, and differences regarding direction and amplitude of nocturnal biases suggest additional factors could have potentially affected LCD temperatures at the three reference sites.

First, the sites differed significantly with regard to parameters influencing micro- and local-scale air temperature variability. At the urban site BOLL, LCD and AWS were placed on the roof of a tall, free-standing building with a sky view factor close to one. Hereby, this site was decoupled from the urban canopy layer and rather representative for dynamics of the roughness sublayer stretching from ground up to two to five times the building height (Oke et al., 2017). Consequently, temperature measurements at this site were probably influenced by processes occurring at larger scales such as wind patterns evolving from topography and regional-scale atmospheric dynamics. This may on the one hand explain the lowest averages of ΔT over the entire study period recorded at this site, because natural ventilation by prevailing wind was arguably most effective given the absence of obstacles such as buildings or trees. Supporting this, mean wind speed throughout the entire study period was highest at BOLL with 1.93 m s^{-1}. On the other hand, the diurnal pattern with a peak of ΔT during daytime hours 9 and 10 (Fig. 3d) could likely be the result of daily cycles in wind patterns (Fig. S2c). These showed a marked increase in wind speed between daytime hours 10 and 11, which may have led to more efficient ventilation and the less pronounced biases during subsequent (afternoon) hours. The underlying cause for these diurnal wind cycles could be attributed to the "shallow Bise", an orographically induced, daily wind pattern typically occurring during summer in the Swiss lowland (Wanner and Furger, 1990). Conversely, wind velocities were significantly reduced at suburban AFU, a site being closely surrounded by buildings up to 39 m and trees. This was reflected in the lowest average wind speed over the entire study period (1.31 m s^{-1}), in lowest maxima of hourly averaged wind speeds, as well as reduced diurnal wind speed variability (Fig. S1b). As a result, surrounding objects likely sheltered the site from prevailing winds and thereby limited natural ventilation of the radiation shield, which may have resulted in the highest mean diurnal ΔT (Table 2), the marked daily amplitude of ΔT (Fig. 3c), and the highest daily maxima of ΔT during the heatwave (Fig. 5a) when compared to the other reference sites. Importantly, this site was probably most representative for the majority of sites of the measurement network being situated in the central and suburban parts of the city. As a consequence, magnitude and temporal patterns of ΔT at many sites were probably similar to those at AFU, which implies potential measurement biases reaching up to 2.5 K during calm and sunny conditions at numerous measurement locations. At rural site ZOLL, which is located within an open field, mean diurnal ΔT was moderate (Table 2) potentially due to relatively unrestricted wind flow with 1.78 m s^{-1} on average over the entire study period. However, a few extreme biases (>2 K) during early evening hours (Fig. 3a) as well as a distinct pattern of predominately positive biases during night-time as well were observed at ZOLL_3m (Fig. 4i). Given that these biases decreased in response to higher wind velocities, limited mixing of air could be a likely source. To control for measurement biases arising from vertical mixing and differing measurement heights, one additional LCD was deployed at 2 m above ground (ZOLL_2m). Intercomparisons between nocturnal temperatures measured at the AWS and the LCD at 2 m showed that positive biases were markedly reduced (Fig. 4j), whereas differences between the LCD at 3 m and the LCD at 2 m were consistently positive (Fig. S1f). This indicates that during nights with low wind speeds, air temperatures were lower at 2 m compared to 3 m above ground, which may be explained by strong radiative cooling of the ground and near-surface air layers leading to a surface-based temperature inversion at rural sites (Oke et al., 2017). Under calm conditions with absent vertical mixing, temperatures therefore decrease with increasing distance from the ground. Due to limited radiative cooling because of restricted horizons (e.g., in street canyons), higher mechanical turbulence, and higher thermal admittance of urban fabrics (Oke et al., 2017), vertical temperature gradients are usually less pronounced in urban environments. As a consequence, differences in measurement heights are supposed to be of less importance at urban and suburban sites (Nakamura and Oke, 1988). However, given that rural reference sites play a key role for many UHI analyses, it is necessary to take into account potential biases arising from different measurement heights (Nakamura and Mahrt, 2005). In addition, our results highlight the importance of conducting parallel measurements at more than one site. By choosing multiple sites for the evaluation of low-cost sensors and radiation shielding designed for the use in urban environments, statements about their performance would be much more robust. With regard to the absence of measurement bias evaluation in many previous UHI studies using naturally ventilated radiation shields (e.g., Svensson and Eliasson, 2002; Schatz and Kucharik, 2015; Smoliak et al., 2015; Skarbit et al., 2017) and bias analyses based on one single reference site (Young et al., 2014), future urban climate studies using low-cost measurement devices should address these shortcomings by providing details about sensor and radiation shield reliability throughout the measurement period.

Second, inter-site differences with regard to the longwave radiation balance could have affected LCD temperature measurements. Longwave radiation fluxes may significantly differ between urban and rural environments with usually higher proportions of incident longwave radiation in urban environments (Oke et al., 2017). Following from this, LCD sensors at the sites BOLL and AFU may have been particularly subject to incident longwave radiation emitted from surrounding objects (e.g., paved surfaces, building walls) that could have resulted in generally higher biases during daytime. During night-time, the emission of longwave radiation dominates the surface radiation balance of the sensor and shield (Nakamura and Mahrt, 2005), which in turn could explain the eventually negative ΔT at night (Fig. 3). As dusring daytime, nocturnal longwave radiation emitted from surrounding urban structures (e.g., streets, buildings) may have impacted the LCD measurements and might thus also explain positive biases found during night-time. However, this process would only be of relevance during clear nights when the longwave radiation balance in urban settings differ significantly from rural settings (Oke et al., 2017). Assuming that the energetic bias introduced by longwave radiation fluxes is equalized by turbulent exchange, reduced ventilation of the LCD radiation shield could have therefore favoured longwave radiative cooling as well as heating, which is supported by our finding reduced variances of ΔT with increasing windspeeds across all three reference sites (Fig. 4i-l).

Third, time lags between the LCD and the AWS measurements could have been responsible for the observed single extreme biases occurring at ZOLL and BOLL during daytime (Fig. 3a, c). One of the main drawbacks of the temperature sensor used in this study was its

relatively long *e*-folding time of 10 min due to a plastic coating. Although raw temperature data sampled at 10 min intervals has been aggregated into hourly averages, rapid changes in air temperature may still have resulted in temporal lags of the LCDs when compared to the quickly responding AWS (5 s). Apart from scattered and broken clouds, such rapid changes may for instance have occurred during or subsequent to precipitation events, where evaporation of water from the falling raindrops could have led to rapid cooling of the ambient air (Byers et al., 1949). Conversely, instantaneous rain downpours quickly followed by sunshine, potentially combined with evaporative cooling of water on the LCD radiation shield or on surrounding surfaces, could have induced rapid warming of the ambient air that could be responsible for negative differences between LCDs and AWS. However, UHI analyses generally focus on periods of clear-sky and dry conditions (Stewart, 2011), which would exclude periods of variable atmospheric conditions related to cloudiness or precipitation events. To overcome measurement biases due to time lags, temperature sensors with shorter *e*-folding (or re times should be used.

Fourth, extreme temperature biases could arise as a result of direct incident solar irradiance on the sensor. This could either be due to low sun angles (Anderson and Baumgartner, 1998) or to the reflection of solar radiation by surface materials with a high albedo (Huwald et al., 2009). Given that the extreme biases found at the reference site were not systematic, that they predominately occurred at low wind speeds, and that none of the reference sites' surfaces were composed of bright materials, we assume the probability of this bias source to be rather low. However, air temperature measurements within specific urban environments (e.g., street canyons, parking spaces) could indeed be subject to radiative biases due to reflected solar radiation from windows, cars, bright urban surfaces, or traffic signs. Therefore, a detailed data quality control with a special focus on physically implausible values is strongly recommended prior to the analysis of urban temperature data.

4.3. Opportunities, challenges, and improvements of the LCD measurement approach

The goal of this study was to evaluate a low-cost approach for high-resolution air temperature measurements in cities. The here presented combination of an inexpensive, self-contained data logger and a custom-made, naturally ventilated radiation shield consisting of widely available components offers several benefits:

First, instrumentation costs for one LCD (~$62 USD) were of similar magnitude (~$61 USD, Hubbart et al. (2005)) or significantly lower than low-cost approaches presented in previous studies (~$150 USD, Young et al. (2014)). The low costs facilitate the acquisition of a multitude of sensors that could enable detailed pictures of spatiotemporal variability of urban air temperatures. Such highly resolved data sets may pave the ground for numerous applications, which include urban climate model evaluations, quality assessments of crowdsourced data, planning and monitoring of heat mitigation options, as well as outreach and education efforts (Chapman et al., 2015). Given that high instrumentation costs may have contributed to the striking underrepresentation of UHI studies from cities in Latin America, Africa, or South Asia (Stewart, 2011), our approach may not only contribute to expanded data coverage, but also to deeper understandings of urban climatology and the development of climate change adaption measures across cities and regions with limited financial resources. In particular with regard to estimated increases in urban population of up to 68% of the world's population by 2050 (United Nations, 2018) and future climate projections pointing towards more frequent, intense, and longer heatwaves (IPCC, 2014), cities in these regions will be facing major challenges regarding adaptation to increasing heat exposure (Bastin et al., 2019).

Second, the self-sufficient and robust temperature logger in combination with its low battery use allowed for continuous measurements and safe storage of data at various time intervals. Although LCD data had to be read out manually and thus cannot be used for real-time applications, chances of missing data and potential sensor failures may be minimized through regular maintenance visits. The issue of interrupted data transmission has been reported by Chapman et al. (2015), whose low-cost temperature sensors transferred data in real-time using municipal Wi-Fi networks. Out of 83 sensors having been installed throughout Birmingham, 73 failed to regularly transmit data due to battery-related problems, server issues, and weak Wi-Fi connections. This underlines the advantages of using independent temperature loggers without major installation restrictions regarding connectivity to networks or power supply. However, the issue of data transmission failures could also be addressed by combining (near) real-time connectivity via Wi-Fi and an internal storage within the same sensor. Such measurement devices would thus integrate the advantages of both technologies and thereby minimize the risk of missing data. Another potential arises from the increasingly implemented and studied data transmission technologies based on long range wide area networks (LoRaWAN; Cotrim and Kleinschmidt, 2020). Due to its relatively low power demand and the growing number of public and open-source gateways, the technology offers various advantages regarding real-time and low-cost measurement approaches of atmospheric parameters in cities (Johnston et al., 2019; Basford et al., 2020).

Third, temperature data recorded by the LCDs during night-time was found to be reliable when compared with automated weather stations (Figs. 3–5). Given that nocturnal heat stress is of similar relevance for human health than thermal stress during the day (Murage et al., 2017), detailed information about night-time UHI intensity may be crucial for the identification of hot spots within urban environments. Based on this, urban planners and municipalities can develop, implement, and monitor options for cooling strategies at variable scales.

However, our results also revealed several shortcomings regarding the use of LCD approach that should be carefully addressed and possibly improved in future studies dealing with low-cost air temperature measurements in urban areas. With regard to the marked measurement biases in situations of high solar irradiance and low wind speeds, active ventilation of the radiation shield could significantly reduce short- and longwave radiative biases of the LCDs. Nevertheless, artificial aspiration requires additional power supply, which may conflict with the choice of appropriate measurement locations and/or instrumentation costs. One possibility to overcome these issues could be the integration of a small, low-voltage fan coupled with a low-cost solar panel, which are available for less than $15 USD. This would allow for at least part-time ventilation of the radiation shield in presence of solar irradiance, which has been shown to significantly reduce radiation biases (Richardson et al., 1999). The development and evaluation of part-time ventilated

air temperature measurement devices could therefore be an important avenue for future research.

Another option to increase quality and reliability of daytime temperature data retrieved by LCDs are corrections of radiative biases based on a combination of modelling and observations. Taking into account parallel measurements of incoming solar irradiance and wind speed, we showed that a simple linear regression modelling approach may explain large portions of the variance of the measurement bias (Table S1). Consequently, similar approaches could be used for bias correction of naturally ventilated radiation shields, which has been demonstrated in previous studies (Anderson and Baumgartner, 1998; Nakamura and Mahrt, 2005). In addition, the inclusion of the radiation shield's geometry (Mauder et al., 2008) and the albedo of the underlying surface (Huwald et al., 2009) has been shown to further improve empirical correction models. However, this approach supposes the existence of observations of wind speed and solar irradiance within close distance to the location of corresponding temperature measurements (Mauder et al., 2008). Given the marked differences of measurement biases we found across the three reference sites (Fig. 3 and 4) and the potentially strong, small-scale heterogeneity of wind patterns and radiation balances in urban environments (Oke et al., 2017), this would imply parallel wind and radiation measurements at a multitude of sites within a city. Thus, future research on low-cost air temperature measurement approaches should focus on this issue by establishing additional meteorological reference sites in different environments with respect to urban metabolism and by conducting intercomparisons of low-cost measurement equipment at these sites. To ensure data quality and the absence of site-specific, systematic biases in the data records, such additional urban reference sites should be operated for at least more than one year (WMO, 2014).

Contrastingly, the number of measurement sites needed for the corrections could be reduced by choosing locations with wind flow and radiation conditions being representative for a variety of urban microclimates. In view of the potentially high instrumentation and maintenance costs associated with that, estimates of local radiation budgets and wind patterns retrieved from micro- and local-scale modelling approaches could provide a cost-effective alternative. A further option would be to use crowd-sourced wind measurements in order to detect times and locations of low wind speeds. However, this would imply improvements in data quality controls given that crowd-sourced wind data seem to be prone to errors in periods of very low wind speeds (Droste et al., 2020). In sum, we aim to highlight the need for stronger efforts regarding the evaluation of low-cost measurement approaches in urban environments to be addressed in future UHI and urban climate studies.

4.4. Applicability of LCD measurement approach for UHI analyses

Apart from evaluating the performance of the LCD approach when directly compared to AWS, we also intended to analyse its suitability for the detection of spatiotemporal UHI characteristics intensities across Bern over the entire study period and during an intense 9-days heatwave. During the heatwave, patterns of ΔT_{UHI} and ΔT were generally in good agreement with regard to the direction and variability of the biases (Fig. 5a-b). However, this is not surprising as ΔT_{UHI} is a function of ΔT at the reference sites, and patterns of ΔT_{UHI} therefore reflect a combination of similar sources for the observed biases. Following from this, daytime UHI intensities derived from LCD temperatures were subject to considerable overestimation (up to 1.8 K) and marked variability likely due to radiative heating and poor ventilation, rapid changes in meteorological conditions, and site-specific characteristics (see discussion above). Conversely, nocturnal UHI magnitudes derived from LCDs underestimated those from AWS by up to 1.1 K, which might be attributed to differences regarding wind speed, the longwave radiation balance, or the measurement height at ZOLL. In summary, the analysis of ΔT_{UHI} showed on the one hand that nocturnal UHI intensities retrieved from LCD temperatures are more reliable than daytime UHI magnitudes. On the other hand, it highlights the importance of not only addressing raw biases for sensor intercomparisons, but also to look at how these biases may translate into a specific application of urban air temperature measurements such as analyses of UHI intensities.

Comparisons between UHI intensities calculated from the LCD measurement network data (Fig. 6a) and those retrieved by the AWS at the two reference sites (AFU and BOLL; Fig. 6b-c) confirmed the assumption of multiple measurement sites being more representative for the intra-urban air temperature variability than by only a few pairs of urban-rural sites (Stewart and Oke, 2012). Although the overall UHI pattern as a function of wind speed as well as the variance of positive UHI intensities was quite well reflected by the two AWS stations, the vast majority of negative UHI intensities' variance was not represented by these. Similarly, analyses of spatial UHI characteristics during the heatwave revealed that the LCD network captured a much wider spectrum of UHI intensities and cooling rates as the LCDs at the two AWS (ZOLL and AFU) only (Fig. 7). In view of the relevance of the detection of local-specific hot and cool spots for urban planning and development (Oke et al., 2017), our results highlight the potential of cost-effective and fine-scaled networks of urban air temperature monitoring sites such as reported here. This holds particularly true for cities with complex topography and small-scale heterogeneity of microclimates, and similar approaches in comparable cities should thus be tackled in future research.

Over the entire study period, nocturnal UHI magnitudes between −6.13 and 6.74 K were registered at the LCD sites of the network (Fig. 6a). Although little work has been published about UHI intensities of Swiss cities (except for Basel: see Parlow et al., 2014 and Wicki et al., 2018), this finding is generally in line with the few previous UHI studies for the city of Bern. Several stationary and mobile air temperature measurement campaigns conducted almost 40 years ago by Wanner and Hertig (1984) revealed maximum temperature differences between urban and rural areas of 5 to 6 K, which peaked between late afternoon and early night. However, comparability with our measurements is limited due to missing information about specific measurement locations and sensor types used. More recently, an analysis of long-term air temperature records (2004–2016) retrieved from pairs of rural and urban weather stations across five Swiss cities reported maximum UHI intensities between 5 and 7 K for Bern during calm summer nights (Gehrig et al., 2018). Similar to our temporal UHI analyses during the heatwave, maximum differences between the city centre and the rural surroundings of Bern during summer were found to occur in early night around 22:00 CET. Despite methodological concerns regarding

direct comparability due to missing details about the different sensor types used, changes in measurement locations, and the ventilation of radiation shields, this supports the plausibility and validity of the UHI intensities observed by the LCD measurement approach. However, taking into account the likely underestimation of nocturnal UHI intensities by the LCDs due to the above-mentioned factors at the rural reference site ZOLL, UHI magnitudes over the entire study period might have even encompassed 7 K.

Although a number of studies found that UHI intensities during periods of extreme heat are as strong or stronger than summer background conditions (e.g., Meir et al., 2013; Li et al., 2015; Schatz and Kucharik, 2015) due to combined effects of hot days coinciding with clear skies, calmer winds, drier soils, and a larger fraction of energy being partitioned into sensible heat (Oke, 1982; Oke et al., 2017), the comparison of LCD-based UHI intensities from the entire study period (−6.13 to 6.74 K; Fig. 6a) with those of the 9-days heatwave (−5.9 to 5.5 K; Fig. 5c) reveals that the synoptic conditions during the heatwave did not reflect the full spectrum of night-time UHI magnitudes of Bern throughout the summer months. Given the considerable variability of ΔT and ΔT_{UHI} we found at the three reference sites during the heatwave (Fig. 5), it may be argued that rapid changes in air temperatures due to sudden shifts of atmospheric background conditions (i.e. wind gusts, precipitation events) at the rural reference site ZOLL could have occasionally resulted in stronger UHI intensities. Another potential explanation for the discrepancy between maximum UHI intensities could be found in local-specific, short-term heat sources (e.g., refrigerated trucks or construction work) situated close to an LCD site within the city. However, the exceptional climatological conditions during the record-dry summer could also have contributed to temporarily higher maximum UHI intensities than measured during the heatwave due to dry soils and subsequent limitations in latent heat fluxes. Following from this, the detection of synoptic conditions and site-specific circumstances leading to maximum UHI intensities reported here would require in-depth analyses and inclusion of additional data sources that could be envisaged in future studies.

Spatial patterns of UHI intensity during the heatwave (Fig. 7a) are in good agreement with what to be expected from theory (Oke, 1982; Oke et al., 2017) and previous studies (see Stewart, 2011 for an overview). Accordingly, higher UHI generally occur in densely-built areas of a city such as the city centre, residential areas, commercial, and industrial districts, whereas temperature differences compared to the rural surroundings are lower in sparsely built and more vegetated parts of city (e.g., parks, forests, suburban residential areas, recreational areas). However, low nocturnal UHI magnitudes along the river channel suggest that local topography likely affected spatial air temperature variability across Bern. As such, cold and dense air masses accumulate within topographical depressions during calm conditions and thereby promote the formation of local inversion layers (Lareau et al., 2013). In the case of Bern, topographical effects on air temperature and UHI patterns are of particular interest due to the distinct river channel crossing the city from southeast to northwest (Wanner and Hertig, 1984). Along the slopes and at the bottom of the channel, major residential projects are being planned within the next decades. With regard to the complex topography of Bern, our results may therefore contribute to the understanding of microclimatic interferences between urban metabolism and topographical features. These could be of special importance for the evaluation and advancement of high-resolution urban climate models being run in cities with heterogeneous topography.

Spatial patterns of cooling rates between late afternoon and early night (Fig. 7b) were generally in good agreement with patterns of UHI intensities. Given that UHI variability depicts the outcome cooling efficiency of near-surface air masses across a city, the two variables are closely related (Oke, 1982). As a consequence, cooling rates may serve as a valuable supplement to enhance the understanding and reliability of observed UHI intensities across a city. However, comparisons of the patterns of the two variables also revealed differences which should be acknowledged in order to draw correct conclusions. As such, cooling rates registered by the LCDs are likely to be overestimated due to the positive measurement biases observed during late afternoon at the reference sites (Fig. 5a). In contrast to this, LCD biases were markedly lower during maximum UHI intensities in early night. Consequently, intercomparisons between cooling rates retrieved by LCDs in Bern and those observed in other cities should be interpreted with caution. Moreover, cooling rates could arguably be more sensitive to effects of local topography and micro-scale urban metabolism. Shadowing effects at low sun angles evolving from the orientation of topographical features (e.g., river channel) or buildings could thereby affect late afternoon air temperatures at small scales and therefore result in different patterns of cooling rates compared to UHI intensities. In summary, our results highlight the potential of cooling rates as valuable, additional source of information for detailed interpretations of local and micro-scale UHI characteristics.

5. Conclusions

The goal of this study was to evaluate the performance and applicability of a cost-effective measurement approach for near-surface air temperatures in urban environments using low-cost, naturally ventilated temperature loggers and custom-made radiation shielding (LCD) for less than $65 USD per device. Intercomparisons with hourly averaged data from three automated, actively ventilated weather stations (AWS) during a period of four months (May 16th until September 15th 2018) revealed predominantly positive biases of the LCDs during daytime ranging from −1.02 to 2.7 K (RMSE: 0.78 to 1.17 K). Analysis of bias sources showed that daytime biases can be explained to a large extent by the amount of solar irradiance and wind speed controlling the degree of radiative heating of the shielding. Linear regression models based on solar irradiance and wind speed were able to explain up to 82.8% of the variance in daytime biases. At night, LCD performance was markedly better with measurement differences varying from −0.68 to 1.27 K and corresponding RMSEs of 0.19 to 0.34 K due to the absence of solar irradiance. Likely affected by the longwave radiation balance of the shields, variances of nocturnal measurement biases were found to decrease in response to higher wind speeds. We conclude that the low-cost measurement approach presented in this study is well suited for nocturnal air temperature measurements within the urban canopy layer, and that bias modelling as well as correction based on wind and radiation data, or part-time ventilation of radiation shielding during daytime could substantially increase data quality from LCDs in cities.

Furthermore, we found biases to be considerably higher at the (sub-)urban compared to the rural reference site, which was very

likely due to reduced wind velocities by surrounding buildings and trees. In view of the fact that the majority of previous sensor and radiation shield intercomparisons were conducted at individual rural sites, our findings on the one hand highlight the need for establishing additional meteorological measurement sites in urban areas. On the other hand, future research should put further emphasis on conducting reference measurements at multiple sites differing in their degree of urban form and metabolism in order to assess the reliability of low-cost air temperature measurements approaches in urban environments. Following from this, previous urban climate studies may have overestimated the performance of naturally ventilated radiation shields, and therefore more emphasis should be put on harmonizing sensor and shielding intercomparisons in realistic urban configurations. Findings of temperature differences regarding different measurement heights at the rural reference site further suggest that the magnitude of late afternoon and nocturnal comparisons between rural and urban temperatures are likely to depend on the choice of measurement height. This was further strengthened by findings of underestimations of nocturnal UHI intensities by the LCDs when compared to AWS measurements and future studies should thus acknowledge this in order to avoid erroneous estimates of nocturnal UHI intensities from low-cost temperature sensors.

In addition to direct intercomparisons with AWS, the presented low-cost approach was applied to detect spatiotemporal UHI patterns during night using a dense network of 79 LCDs across Bern over the entire study period as well as during an intense 9-days heatwave (July 30th until August 7th 2018). In accordance with theory and previous studies, we found UHI intensities of −6.13 to 6.74 K over the entire study period, which markedly expanded the range of UHI variability captured by the existing AWS. During the heatwave, maximum UHI intensities of up to 5.5 K occurred during late evening (22:00 CET) and in the city centre as well as in densely built commercial districts and residential areas. The heterogeneous terrain of the city resulted in considerable micro- to local-scale variability of nocturnal air temperatures, which was reflected in both, patterns of UHI intensity and cooling rates. Our findings proved the applicability of the LCD measurement approach in assessing nocturnal UHI characteristics and may contribute to the development and validation of high-resolution urban climate modelling approaches for cities located in complex terrain.

In sum, the low-cost measurement approach for air temperatures within the urban canopy layer presented here may be of great value in gaining a deeper understanding of urban climate dynamics at regional to micro-scales. Especially in cities with restricted financial resources, the LCD approach represents a valuable and cost-effective tool with considerable potential in assisting the development, appliance, and monitoring of adaptation strategies to current and future climate change.

Data availability

The raw data sets used for the analyses can be accessed and downloaded from: https://boris.unibe.ch/id/eprint/140420

Author contributions

MG led the conceptualization of the study, wrote the original draft, revised and edited it. SB, JR, and AC contributed to the conceptualization, commented on and refined all versions of the manuscript.

Funding sources

This research did not receive any specific grant from funding agencies in the public, commercial, or not-for-profit sectors.

Declaration of Competing Interest

The authors declare that they have no conflict of interest.

Acknowledgements

This paper is dedicated to Hans Kallen, former technician of the Geographical Institute of the University of Bern, who passed away unexpectedly in late 2018. Without his precious help in designing and refining the low-cost measurement devices, this study would not have been possible. Further, we are very thankful to teaching assistant Lukas Meyer for helping with the construction of the LCDs and with field work. We also would like to thank the numerous authorities, companies, and experts from the city of Bern for their permissions granted to deploy the LCDs and their constructive comments during the planning phase of the network. Finally, we would like to thank the two anonymous reviewers for their helpful comments on an earlier version of this manuscript.

Appendix A. Supplementary data

Supplementary data to this article can be found online at https://doi.org/10.1016/j.uclim.2021.100817.

References

Anderson, S., Baumgartner, M., 1998. Radiative heating errors in naturally ventilated air temperature measurements made from buoys. J. Atmos. Ocean. Technol. 15, 157–173. https://doi.org/10.1175/1520-0426.

Auchmann, R., Brönnimann, S., 2012. A physics-based correction model for homogenizing sub-daily temperature series. J. Geophys. Res.-Atmos. 117, D17119 https://doi.org/10.1029/2012jd018067.

AVR: Amtliche Vermessung Reduziert (EN: "Reduced Cadastral Survey"), Office for Geoinformation of the Canton of Bern, https://files.be.ch/bve/agi/geoportal/geo/lpi/AVR_2011_03_LANG_DE.PDF (last visited: 01/17/2021), 2015 .

Basford, P.J., Bulot, F.M.J., Apetroaie-Cristea, M., Cox, S.J., Ossont, S.J., 2020. LoRaWAN for Smart City IoT deployments: a long term evaluation. Sensors 20, 648. https://doi.org/10.3390/s20030648.

Bastin, J.-F., Clark, E., Elliott, T., Hart, S., van den Hoogen, J., Hordijk, I., Ma, H., Majumder, S., Manoli, G., Maschler, J., Mo, L., Routh, D., Yu, K., Zohner, C.M., Crowther, T.W., 2019. Understanding climate change from a global analysis of city analogues. PLoS One 14, e0217592. https://doi.org/10.1371/journal.pone.0217592.

Bell, S., Cornford, D., Bastin, L., 2015. How good are citizen weather stations? Addressing a biased opinion. Weather 70, 75–84. https://doi.org/10.1002/wea.2316.

Burton, B., 2014. Stevenson screen temperatures – an investigation. Weather 69, 156–160. https://doi.org/10.1002/wea.2166.

Byers, H.R., Moses, H., Harney, P.J., 1949. Measurement of rain temperature. J. Meteorol. 6, 51–55. https://doi.org/10.1175/1520-0469.

Chapman, L., Muller, C.L., Young, D.T., Warren, E.L., Grimmond, C.S.B., Cai, X.-M., Ferranti, E.J.S., 2015. The Birmingham urban climate laboratory: an open meteorological test bed and challenges of the smart city. B. Am. Meteorol. Soc. 96, 1545–1560. https://doi.org/10.1175/bams-d-13-00193.1.

Chapman, L., Bell, C., Bell, S., 2017. Can the crowdsourcing data paradigm take atmospheric science to a new level? A case study of the urban heat island of London quantified using Netatmo weather stations. Int. J. Climatol. 37, 3597–3605. https://doi.org/10.1002/joc.4940.

Cotrim, J.R., Kleinschmidt, J.H., 2020. LoRaWAN mesh networks: a review and classification of multihop communication. Sensors 20, 4273. https://doi.org/10.3390/s20154273.

Droste, A.M., Heusinkveld, B.G., Fenner, D., Steeneveld, G.-J., 2020. Assessing the potential and application of crowdsourced urban wind data. Q. J. R. Meteorol. Soc. 146, 2671–2688. https://doi.org/10.1002/qj.3811.

EEA, 2012. Copernicus Land Monitoring Service – Urban Atlas, European Environmental Agency. https://land.copernicus.eu/local/urban-atlas.

Esri, 2019. ArcGIS Pro (version 2.4.0). Environmental Systems Research Institute, Redlands, CA.

Fenner, D., Meier, F., Bechtel, B., Otto, M., Scherer, D., 2017. Intra and inter 'local climate zone' variability of air temperature as observed by crowdsourced citizen weather stations in Berlin, Germany. Meteorol. Z. 26, 525–547. https://doi.org/10.1127/metz/2017/0861.

Fenner, D., Holtmann, A., Meier, F., Langer, I., Scherer, D., 2019. Contrasting changes of urban heat island intensity during hot weather episodes. Environ. Res. Lett. 14, 124013. https://doi.org/10.1088/1748-9326/ab506b.

FINBE, 2018. Resident Population of Municipalities, Administrative Districts and Administrative Regions on 12/31/2017. Financial Administration of the Canton of Bern, Bern.

Gehrig, R., König, N., Scherrer, S., 2018. Städtische Wärmeinseln in der Schweiz - Klimatologische Studie mit Messdaten in fünf Städten (EN: "Urban heat islands in Switzerland – Climatological study with measurement data in five cities"), MeteoSwiss technical report, 273 (61 pp.).

Ginzler, C., Hobi, M.L., 2015. Countrywide stereo-image matching for updating digital surface models in the framework of the Swiss national forest inventory. Remote Sens.-Basel 7, 4343–4370. https://doi.org/10.3390/rs70404343.

Grimmond, C.S.B., 2006. Progress in measuring and observing the urban atmosphere. Theor. Appl. Climatol. 84, 3–22. https://doi.org/10.1007/s00704-005-0140-5.

Gubler, M., Henne, P.D., Schwörer, C., Boltshauser-Kaltenrieder, P., Lotter, A.F., Brönnimann, S., Tinner, W., 2018. Microclimatic gradients provide evidence for a glacial refugium for temperate trees in a sheltered hilly landscape of northern Italy. J. Biogeogr. 45, 2564–2575. https://doi.org/10.1111/jbi.13426.

Hubbart, J., Link, T., Campbell, C., Cobos, D., 2005. Evaluation of a low-cost temperature measurement system for environmental applications. Hydrol. Process. 19, 1517–1523. https://doi.org/10.1002/hyp.5861.

Huwald, H., Higgins, C., Boldi, M.-O., Bou-Zeid, E., Lehning, M., Parlange, M., 2009. Albedo effect on radiative errors in air temperature measurements. Water Resour. Res. 45, W08431 https://doi.org/10.1029/2008WR007600.

IPCC, 2014. Climate Change 2014: Synthesis Report. Contribution of Working Groups I, II and III to the Fifth Assessment Report of the Intergovernmental Panel on Climate Change. IPCC, Geneva, Switzerland (151 pp.).

Johnston, S.J., Basford, P.J., Bulot, F.M.J., Apetroaie-Cristea, M., Easton, N.H.C., Davenport, C., Foster, G.L., Loxham, M., Morris, A.K.R., Cox, S.J., 2019. City scale particulate matter monitoring using LoRaWAN based air quality IoT devices. Sensors 19, 209. https://doi.org/10.3390/s19010209.

Lareau, N.P., Crosman, E., Whiteman, C.D., Horel, J.D., Hoch, S.W., Brown, W.O.J., Horst, T.W., 2013. The persistent cold-air pool study. B. Am. Meteorol. Soc. 94, 51–63. https://doi.org/10.1175/bams-d-11-00255.1.

Li, D., Sun, T., Liu, M., Yang, L., Wang, L., Gao, Z., 2015. Contrasting responses of urban and rural surface energy budgets to heat waves explain synergies between urban heat islands and heat waves. Environ. Res. Lett. 10, 054009 https://doi.org/10.1088/1748-9326/10/5/054009.

Lin, X., Hubbard, K.G., Walter-Shea, E.A., Brandle, J.R., Meyer, G.E., 2001. Some perspectives on recent in situ air temperature observations: modeling the microclimate inside the radiation shields. J. Atmos. Ocean. Technol. 18, 1470–1484. https://doi.org/10.1175/1520-0426.

Lindberg, F., Grimmond, C.S.B., Gabey, A., Huang, B., Kent, C.W., Sun, T., Theeuwes, N.E., Järvi, L., Ward, H.C., Capel-Timms, I., Chang, Y., Jonsson, P., Krave, N., Liu, D., Meyer, D., Olofson, K.F.G., Tan, J., Wästberg, D., Xue, L., Zhang, Z., 2018. Urban multi-scale environmental predictor (UMEP): an integrated tool for city-based climate services. Environ. Model. Softw. 99, 70–87. https://doi.org/10.1016/j.envsoft.2017.09.020.

Matese, A., Gennaro, S.F.D., Zaldei, A., Genesio, L., Vaccari, F.P., 2009. A wireless sensor network for precision viticulture: the NAV system. Comput. Electron. Agric. 69, 51–58. https://doi.org/10.1016/j.compag.2009.06.016.

Mauder, M., Desjardins, R.L., Gao, Z., Haarlem, R.V., 2008. Errors of naturally ventilated air temperature measurements in a spatial observation network. J. Atmos. Ocean. Technol. 25, 2145–2151. https://doi.org/10.1175/2008jtecha1046.1.

Meier, F., Fenner, D., Grassmann, T., Jänicke, B., Otto, M., Scherer, D., 2017. Crowdsourcing air temperature from citizen weather stations for urban climate research. Urban Clim. 19, 170–191. https://doi.org/10.1016/j.uclim.2017.01.006.

Meir, T., Orton, P.M., Pullen, J., Holt, T., Thompson, W.T., Arend, M.F., 2013. Forecasting the New York City urban heat island and sea breeze during extreme heat events. Weather Forecast. 28, 1460–1477. https://doi.org/10.1175/waf-d-13-00012.1.

Meteolabor, 2019. Data-sheet for Thygan thermo-hygrometer VTP37, Meteolabor, Wetzikon, Switzerland.

MeteoSwiss, 2017. Climate Normals Bern/Zollikofen, Federal Office of Meteorology and Climatology MeteoSwiss, Zurich.

MeteoSwiss, 2018. Hitze und Trockenheit im Sommerhalbjahr 2018 - eine klimatologische Übersicht (EN: "Heat and drought during summer half-year – a climatological overview"), MeteoSwiss Technical Report, 272 (38 pp.).

van der Meulen, J.P., Brandsma, T., 2008. Thermometer screen intercomparison in De Bilt (The Netherlands), Part I: understanding the weather-dependent temperature differences. Int. J. Climatol. 28, 371–387. https://doi.org/10.1002/joc.1531.

Milan, B.F., Creutzig, F., 2015. Reducing urban heat wave risk in the 21st century. Curr. Opin. Environ. Sustain. 14, 221–231. https://doi.org/10.1016/j.cosust.2015.08.002.

Muller, C.L., Chapman, L., Grimmond, C.S.B., Young, D.T., Cai, X.-M., 2013a. Toward a standardized metadata protocol for urban meteorological networks. B. Am. Meteorol. Soc. 94, 1161–1185. https://doi.org/10.1175/bams-d-12-00096.1.

Muller, C.L., Chapman, L., Grimmond, C.S.B., Young, D.T., Cai, X.-M., 2013b. Sensors and the city: a review of urban meteorological networks. Int. J. Climatol. 33, 1585–1600. https://doi.org/10.1002/joc.3678.

Murage, P., Hajat, S., Kovats, S., 2017. Effect of night-time temperatures on cause and age-specific mortality in London. Adv. Chem. Ser. 1, e005 https://doi.org/10.1097/EE9.0000000000000005.

Nakamura, R., Mahrt, L., 2005. Air temperature measurement errors in naturally ventilated radiation shields. J. Atmos. Ocean. Technol. 22, 1046–1058. https://doi.org/10.1175/jtech1762.1.
Nakamura, Y., Oke, T.R., 1988. Wind, temperature and stability conditions in an east-west oriented urban canyon. Atmos. Environ. (1967) 22, 2691–2700. https://doi.org/10.1016/0004-6981(88)90437-4.
Napoly, A., Grassmann, T., Meier, F., Fenner, D., 2018. Development and application of a statistically-based quality control for crowdsourced air temperature data. Front. Earth Sci. 6 https://doi.org/10.3389/feart.2018.00118.
Oke, T.R., 1982. The energetic basis of the urban heat island. Q. J. Roy. Meteorol. Soc. 108, 1–24. https://doi.org/10.1002/qj.49710845502.
Oke, T.R., Mills, G., Christen, A., Voogt, J.A., 2017. Urban Climates. Cambridge University Press, Cambridge. https://doi.org/10.1017/9781139016476 (526 pp.).
Onset, 2013. HOBO UA-001-08 Data Logger Specifications. Onset Computer Corporation.
Parlow, E., Vogt, R., Feigenwinter, C., 2014. The urban heat island of Basel - seen from different perspectives. Erde 145, 96–110. https://doi.org/10.12854/erde-145-8.
QGIS Development Team, 2019. QGIS Geographic Information System (Version 3.2.1-Bonn). Open Source Geospatial Foundation Project. http://qgis.osgeo.org/.
R Core Team, 2019. R: A Language and Environment for Statistical Computing. R Foundation for Statistical Computing, Vienna, Austria. https://www.r-project.org/.
Richardson, S.J., Brock, F.V., Semmer, S.R., Jirak, C., 1999. Minimizing errors associated with multiplate radiation shields. J. Atmos. Ocean. Technol. 16, 1862–1872. https://doi.org/10.1175/1520-0426(1999)016<1862:MEAWMR>2.0.CO;2.
Schatz, J., Kucharik, C.J., 2015. Urban climate effects on extreme temperatures in Madison, Wisconsin, USA. Environ. Res. Lett. 10, 094024 https://doi.org/10.1088/1748-9326/10/9/094024.
Skarbit, N., Stewart, I.D., Unger, J., Gál, T., 2017. Employing an urban meteorological network to monitor air temperature conditions in the 'local climate zones' of Szeged, Hungary. Int. J. Climatol. 37, 582–596. https://doi.org/10.1002/joc.5023.
Smoliak, B.V., Snyder, P.K., Twine, T.E., Mykleby, P.M., Hertel, W.F., 2015. Dense network observations of the twin cities canopy-layer urban heat island. J. Appl. Meteorol. Climatol. 54, 1899–1917. https://doi.org/10.1175/jamc-d-14-0239.1.
Stewart, I.D., 2011. A systematic review and scientific critique of methodology in modern urban heat island literature. Int. J. Climatol. 31, 200–217. https://doi.org/10.1002/joc.2141.
Stewart, I.D., Oke, T.R., 2012. Local climate zones for urban temperature studies. B. Am. Meteorol. Soc. 93, 1879–1900. https://doi.org/10.1175/bams-d-11-00019.1.
Svensson, M.K., Eliasson, I., 2002. Diurnal air temperatures in built-up areas in relation to urban planning. Landsc. Urban Plan. 61, 37–54. https://doi.org/10.1016/S0169-2046(02)00076-2.
Swisstopo, 2017. High Precision Digital Elevation Model of Switzerland (swissALTI^{3D}) and High Precision Building Model of Switzerland (swissBUILDINGS3D 2.0). Federal Office of Topography swisstopo.
Tarara, J.M., Hoheisel, G.-A., 2007. Low-cost shielding to minimize radiation errors of temperature sensors in the field. Hortic. Sci. 42, 1372–1379. https://doi.org/10.21273/hortsci.42.6.1372.
Terando, A.J., Youngsteadt, E., Meineke, E.K., Prado, S.G., 2017. Ad hoc instrumentation methods in ecological studies produce highly biased temperature measurements. Ecol. Evol. 7, 9890–9904. https://doi.org/10.1002/ece3.3499.
United Nations: World Urbanization Prospects: The 2018 Revision [key facts], United Nations' Department of Economic and Social Affairs: Population Dynamics, https://population.un.org/wup/Publications/Files/WUP2018-KeyFacts.pdf (last visited: 01/17/2021), 2018.
Vogel, M.M., Zscheischler, J., Wartenburger, R., Dee, D., Seneviratne, S.I., 2019. Concurrent 2018 hot extremes across northern hemisphere due to human-induced climate change. Earths Future 7, 692–703. https://doi.org/10.1029/2019ef001189.
Wanner, H., Furger, M., 1990. The Bise – climatology of a regional wind north of the Alps. Meteorog. Atmos. Phys. 43, 105–115. https://doi.org/10.1007/bf01028113.
Wanner, H., Hertig, J.-A., 1984. Studies of urban climates and air pollution in Switzerland. J. Clim. Appl. Meteorol. 23, 1614–1625. https://doi.org/10.1175/1520-0450(1984)023<1614:Soucaa>2.0.Co;2.
Ward, K., Lauf, S., Kleinschmit, B., Endlicher, W., 2016. Heat waves and urban heat islands in Europe: a review of relevant drivers. Sci. Total Environ. 569–570, 527–539. https://doi.org/10.1016/j.scitotenv.2016.06.119.
Wicki, A., Parlow, E., Feigenwinter, C., 2018. Evaluation and modeling of urban Heat Island intensity in Basel, Switzerland. Climate 6, 55. https://doi.org/10.3390/cli6030055.
WMO, 2006. Initial Guidance to Obtain Representative Meteorological Observations at Urban Sites. World Meteorological Organization, Geneva (47 pp.).
WMO, 2014. Guide to Meteorological Instruments and Methods of Observation. World Meteorological Organization, Geneva (1177 pp.).
Young, D.T., Chapman, L., Muller, C.L., Cai, X.-M., Grimmond, C.S.B., 2014. A low-cost wireless temperature sensor: evaluation for use in environmental monitoring applications. J. Atmos. Ocean. Technol. 31, 938–944. https://doi.org/10.1175/jtech-d-13-00217.1.
Zhou, D., Xiao, J., Bonafoni, S., Berger, C., Deilami, K., Zhou, Y., Frolking, S., Yao, R., Qiao, Z., Sobrino, J., 2019. Satellite remote sensing of surface urban heat islands: Progress, challenges, and perspectives. Remote Sens.-Basel 11, 36. https://doi.org/10.3390/rs11010048.